# FINAL TECHNICAL REPORT

## AN INTEGRATED GEOPHYSICAL ASSESSMENT OF LATE QUATERNARY NEOTECTONICS ALONG THE NORTHER MISSISSIPPI EMBAYMENT EXTENSION OF THE FLUORSPAR AREA FAULT COMPLEX

**Award Number: 01HQGR0044**

Principal Investigator: Edward W. Woolery

Department of Geological Sciences/
Kentucky Geological Survey
University of Kentucky
101 Slone Research Building
Lexington, KY 40506-0053
Phone: 859.257.3016
Fax: 859.257.1147
Email: woolery@uky.edu
http://www.uky.edu/KGS/

Co-PI: Ron L. Street

Kentucky Geological Survey
228 Mining and Mineral Resources Building
Lexington, KY 40506-0107
Phone: 859.257.5500

Program Element: CU/I
Key Words: Neotectonics, Tectonophysics, Quaternary Fault Behavior

Award Number: 01HQGR0044

# AN INTEGRATED GEOPHYSICAL ASSESSMENT OF LATE QUATERNARY NEOTECTONICS ALONG THE NORTHER MISSISSIPPI EMBAYMENT EXTENSION OF THE FLUORSPAR AREA FAULT COMPLEX

Edward W. Woolery[1], Ron Street[2], and Zhenming Wang[2], *Dept. of Geological Sciences[1], Kentucky Geological Survey[2], University of Kentucky, 101 Slone Bldg., Lexington, Ky. 40506-0053, Tel: 859.257.3016, Fax: 859.257.1147, Email: woolery@uky.edu*

**ABSTRACT**

Shallow seismic-reflection and ground-penetrating radar (GPR) profiles were collected over the southwestern projection of the Fluorspar Area Fault Complex into the northern Jackson Purchase Region of western Kentucky. The study was focused in two areas (eastern and western) that lie at the northern end of the sediment-filled Mississippi Embayment where the Paleozoic carbonate rocks are masked by a relatively thin, approximately 100 m sequence of unlithified Cretaceous, Tertiary, and Quaternary sediments. The interpreted geophysical profiles imaged clear evidence of fault and apparent fold propagation into the near-surface Quaternary units. The profiles also showed evidence of various structural styles associated with episodic movement.

In addition, indirect and direct geotechnical measurements from engineering investigations in the western area have revealed the presence of high lateral earth pressure ($K_o$) in shallow, unlithified sediment. Results from pile-load and pressuremeter tests showed maximum $K_o$ values greater than 10; however, the complex geologic environment of the Midcontinent made defining an origin for the anomalous $K_o$ based solely on these measurements equivocal. Although in situ sediment characteristics indicated that indirect tectonic or nontectonic geologic mechanisms that include transient overburden loads (e.g., fluvial deposition/erosion, glacial advance/retreat) and dynamic shear loads (e.g., earthquakes) were not the dominant cause, they were unable to provide indicators for a direct tectonic generation. Localized stresses induced anthropogenically by the geotechnical field tests were also considered, but ruled out as the primary origin. High-resolution seismic reflection and GPR images of geologic structure in the immediate vicinity of the geotechnical test site revealed compression-style neotectonism, and suggested the elevated stress was a tectonic manifestation. Post-Paleozoic reflectors exhibit a Tertiary (?) structural inversion, as evidenced by post-Cretaceous fault displacement and pronounced positive folds in the hanging wall of the interpreted faults. The latest stratigraphic extent of the stress effects (i.e., all measurements were in the Late Cretaceous to Tertiary McNairy Formation), as well as the relationship of stress orientation with the orientation of local structure and regional stress, remains unknown. These will be the topics of follow-up studies.

The exact timing of the latest tectonic episode exhibited in the dataset is unknown because of the lack of more accurate stratigraphic detail coincident with the profiles. However, physical evidence of Quaternary deformation less than 10 m below the ground surface emphasizes the problematic nature of these fault segments for the design of critical or high-hazard structures.

## 2.0 NONTECHNICAL SUMMARY

Subsurface images of deformed sediments within the northern Mississippi embayment are providing direct physical evidence of relatively recent tectonic activity. The images are enabling researchers to estimate the time of movement, as well as, to understand the style and geometry of the deformation. Results have shown that deformation extends to within at least 7 meters of the ground surface. Preliminary age estimates suggest that the movement occurred between 75,000 and 135,000 BP.

There are limitations to the resolving power of each geophysical technique used; consequently, the exact timing of the latest tectonic episode at some locations is uncertain. In these instances, we hope to coordinate with, and provide target information to, researchers specializing in trenching/paleoseismology.

## 3.0 INTRODUCTION

Accurate identification and characterization of near-surface geologic structures in the expansive river valleys of the seismically active central United States is often impeded by relatively thick sequences of nonlithified, water-saturated sediment. The soft sediment cover conceals neotectonic bedrock structure and, apart from a few notable exceptions (i.e., Crowley's Ridge, Reelfoot Scarp, Commerce Fault, and possibly Sikeston Ridge), the sediment's inherently weak mechanical properties commonly fail to transform near-surface propagated faults and folds into significant or noticeable surface geomorphic features. The northern Jackson Purchase Region of western Kentucky is typical of this setting (Fig. 1). It lies at the central juncture of two late Precambrian–early Paleozoic rifts, the Reelfoot Rift and the Rough Creek Graben (Kolata and Nelson, 1991), as well as near the northern end of the sediment-filled Mississippi Embayment. Immediately north of the Jackson Purchase, in southern Illinois, is the intensely faulted Fluorspar Area Fault Complex that Nelson et al. (1997, 1999) described as a series of strike-slip pull-apart grabens bounded by N20°E- to N40°E-striking normal and reverse faults (Fig. 1). In the Jackson Purchase, the Paleozoic bedrock is covered by several tens to a few hundred meters of Late Cretaceous and younger sediments. Wheeler et al. (1997), as well as Kolata and Nelson (1991), suggested the continuation of the fault complex into this area, but their evidence is primarily inferred from a north–south-oriented, low-resolution, proprietary seismic-reflection profile (J. Drahovzal, oral commun., 1998). More recently, the geologic data gathered by Nelson et al. (1999) and McBride et al. (2002) substantiate faults at least as far south as the Ohio River in Illinois.

Olive (1980) mapped a few faults in Tertiary and Quaternary deposits in the area, but stated that these structures were based on indirect evidence and possibly attributable to non-tectonic mechanisms. Subsequently, until Langston et al.'s (1998) study west of Paducah, Ky., which focused on the structural control of local ground-water movement, there has been no systematic effort to delineate the inferred extension of the fault complex into western Kentucky's Jackson Purchase. Because of the lack of geomorphic surface signatures indicative of subsurface structure, initial reflection profiles in the eastern study area were sited based on large anomalies seen in a low-resolution "sparker" survey conducted for the U.S. Army Corps of Engineers along the Ohio River (Alpine Geophysical Associates Inc., 1966) (Fig. 2). A 710 m SH-wave seismic-reflection profile (UK-B3) from Langston et al.'s (1998) work, and a recently acquired 400 m high-resolution SH-wave CDP profile (UK-H2), provide evidence for the southwestern continuation (Fig. 2). In addition to the spatial extension for the faults, the most recent data show evidence of displacement and disruption of reflectors in the very near surface (~ 7 m).

In the western study area, during foundation design investigations for a U.S. Army Corps of Engineers navigation structure on the lower Ohio River (Olmsted Locks and Dam), geotechnical indicators of elevated lateral earth pressures were discovered in unlithified, near-surface (< 50 m), Cretaceous sediment (Figure 3) (Schaefer, 2001). The magnitude of the lateral earth pressure, a direct result of horizontal stresses in the sediment, was characterized by a series of pile-load and pressuremeter tests; however, the source of the anomalous measurements was equivocal. Localized geologic force variations (i.e., thermal anomalies, crustal loading, and structure heterogeneity) control the actual stress magnitude and orientation, as well as the scale at which stress characteristics are exhibited (Badawy, 2001). Determining the source of the in

situ stress field within the near-surface unlithified sediment was also complicated by various nontectonic and indirect-tectonic geologic mechanisms that include transient overburden loads (e.g., fluvial deposition/erosion, glacial advance/retreat) and dynamic shear loads (e.g., earthquakes), respectively. Localized stresses induced anthropogenically by the geotechnical field tests were also possible, and was considered.

The characteristics of the affected geologic horizons can act as a potential indicator of stress origin. Evidence of geologic structure at the project site was first documented during the initial subsurface foundation investigations. Seismic-refraction and drill-hole data indicated deformation extending into the post-Paleozoic sediment (Yule and Sharp, 1988; Schaefer, 2001). Consequently, as part of integrated geophysical program designed to assess possible neotectonic deformation, a shallow, high-resolution, seismic-reflection and GPR profiles were acquired along the river's shoreline, across the area of suspected geologic structure. The primary objectives for the Olmsted survey were to address two questions: (1) do local geologic structures at the site exhibit neotectonism and (2) if neotectonic deformation is present, can the style of deformation be used to infer an origin for the high horizontal stresses observed in the geotechnical tests. We believed an integrated assessment of the geotechnical and geophysical datasets could sufficiently constrain the stress origin.

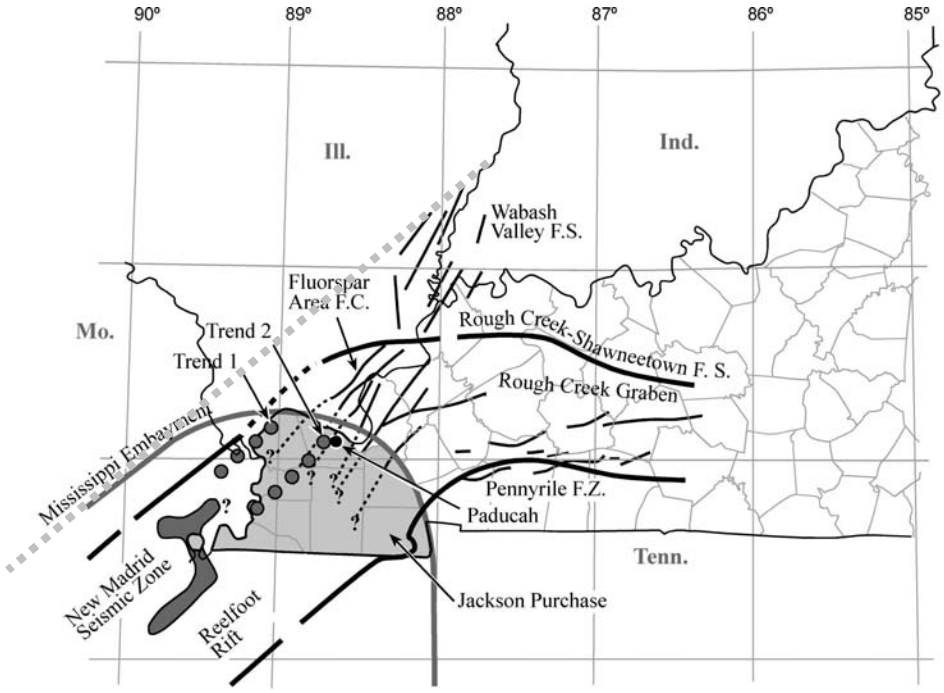


**Figure 1. Major structural features in the central Mississippi Valley (modified from Kolata and Nelson, 1997). The lines of shaded circles represent the locations of Wheeler's (1997) trends 1 and 2 seismicity in relation to the New Madrid seismic zone and the study area. The light gray dashed line indicates the Commerce Geophysical Lineament. The Jackson Purchase Region of western Kentucky is also identified**.

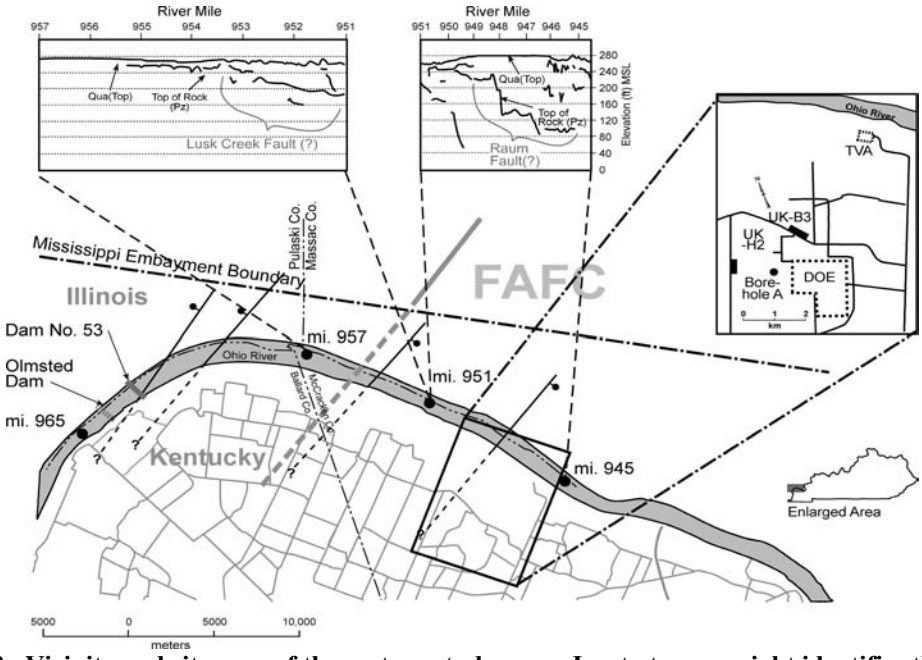


**Figure 2. Vicinity and site map of the eastern study area. Inset at upper right identifies the specific location of SH-wave reflection profiles and geotechnical borehole. The two panels across the top show the large anomalies in the Corps of Engineers "sparker" profiles between river miles 940 and 957 (modified from Alpine Geophysical Associates, Inc., 1966). The solid lines with barbs and balls identify the major offsets seen in the "sparker" data. The balls are placed on the downthrown side. The Fluorspar Area fault complex (FAFC) is defined by the thick, NE-trending solid and dashed line. The gray network of lines in Kentucky and the thin, black network of lines in the inset represent the local highways.**

## 4.0 GEOLOGIC SETTING AND GEOTECHNICAL CHARACTERISTICS

There is a lack of scientific consensus regarding the complex structural relationship between the Reelfoot Rift, the most seismically active of the central and eastern United States rifts, and the Rough Creek Graben, one of the least active major structures (Wheeler, 1997; Street et al., *this volume*). The Rough Creek Graben, which lies mainly in western Kentucky, is bounded on the north by the Rough Creek–Shawneetown Fault System and on the south by a series of faults that include the Pennyrile Fault System (Fig. 1). The Rough Creek–Shawneetown Fault System extends from Kentucky into southern Illinois for about 25 km, then turns abruptly to the southwest and joins the Lusk Creek and Raum fault zones, which form the northwestern boundary of the Fluorspar Area Fault Complex (Nelson and Lumm, 1987). The fault complex is believed to continue southwest across the Jackson Purchase of western Kentucky, beneath sedimentary cover of the northern Mississippi Embayment, where it appears to form the northwest margin of the Reelfoot Rift, the host geologic structure of the New Madrid Seismic Zone (Kolata and Nelson, 1991). This interpretation is supported by potential field data (Hildenbrand and Hendricks, 1995). The faults that make up the fault complex are thought to have originated in the Cambrian; some exhibit evidence of multiple episodes of dip-slip, as well as strike-slip movement into the Quaternary (Nelson et al., 1999). Nelson et al. (1999) found evidence of Pliocene to early Pleistocene displacement along the Lusk Creek Fault Zone in southern Illinois, although they saw no instance of Holocene sediment displacement. Holocene sediments were also found undisturbed in their observations of the neighboring Raum Fault.

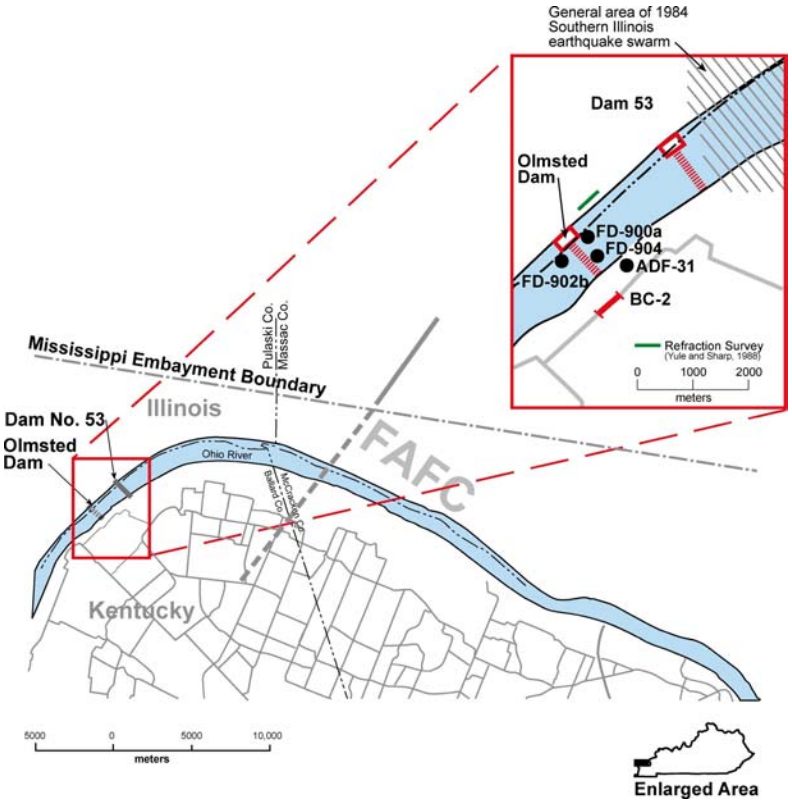


**Figure 3. Vicinity and site map of the western study area. Inset at upper right identifies the location of SH-wave reflection profile (BC-2) and geotechnical test holes. Boreholes FD-900a, 902b, and 904 were locations of pressuremeter tests, and ADF-31was the site of cross-hole velocity and stratigraphy study (Schaefer, 2001). The pile-load tests were all performed inside the open rectangle representing the Olmsted lock chamber. The Fluorspar Area fault complex (FAFC) is defined by the thick, NE-trending, solid and dashed gray line. The gray network of thin lines in Kentucky and the inset represent the local roadways.**

## 4.1 Eastern Study Area

The eastern study area is located along the Ohio River, approximately 10 km west of Paducah, Ky., and near the northern end of the Mississippi Embayment (Fig. 2). The area is also situated near Wheeler's (1997) "trend 2" projection of New Madrid seismicity (Fig. 1). The post-Paleozoic stratigraphy for the area is shown in Figure 4. The Mississippian limestone bedrock is unconformably overlain by approximately 100 m of nonlithified sediments of Late Cretaceous, Paleocene, Eocene, Pliocene, Pleistocene, and Holocene age (Olive, 1980). Late Cretaceous gravel and sand associated with the Tuscaloosa Formation or undifferentiated Late Cretaceous and Paleocene interbedded sands and clays belonging to the McNairy and Clayton Formations rest directly on the bedrock. The McNairy-Clayton Formations are overlain by the Paleocene, montmorillonitic (locally glauconitic) Porters Creek Clay. Undifferentiated Eocene silty sands and clays unconformably overlie the Porters Creek Clay. The Eocene sands and clays are separated from the Pleistocene loess by Pliocene–Pleistocene sands and gravels, locally referred to as the Continental Deposits. Above the continental sands and gravels is Pleistocene loess. The loess is composed primarily of silt intermixed with minor amounts of clay and fine sand. The stratigraphic column is capped by Pleistocene and Holocene silt, sand, and gravel deposits.

We interpreted four consistent reflectors across the study area, identified R1 to R4 on Figures 4 and 5.

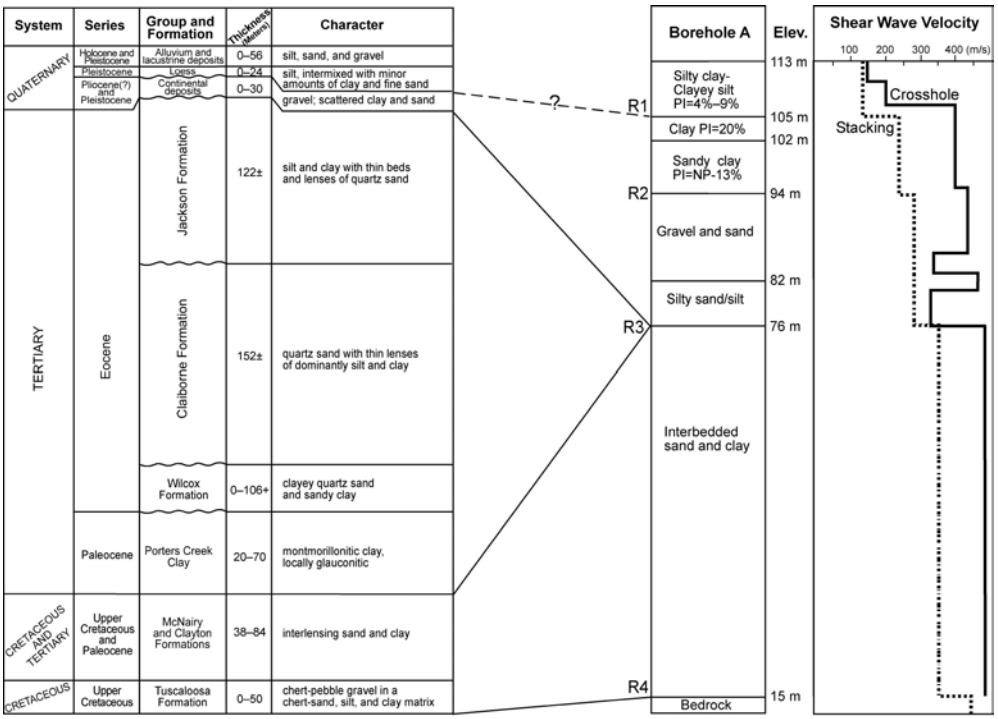


**Figure 4. Local stratigraphy and interpreted correlation to the nearby geotechnical Borehole A (modified from Olive, 1980; Sykora and Davis, 1993). The plasticity indices (PI) are given as a range of moisture contents between the soil's plastic and liquid limits. NP defines a non-plastic soil, (i.e., sand or gravel).**

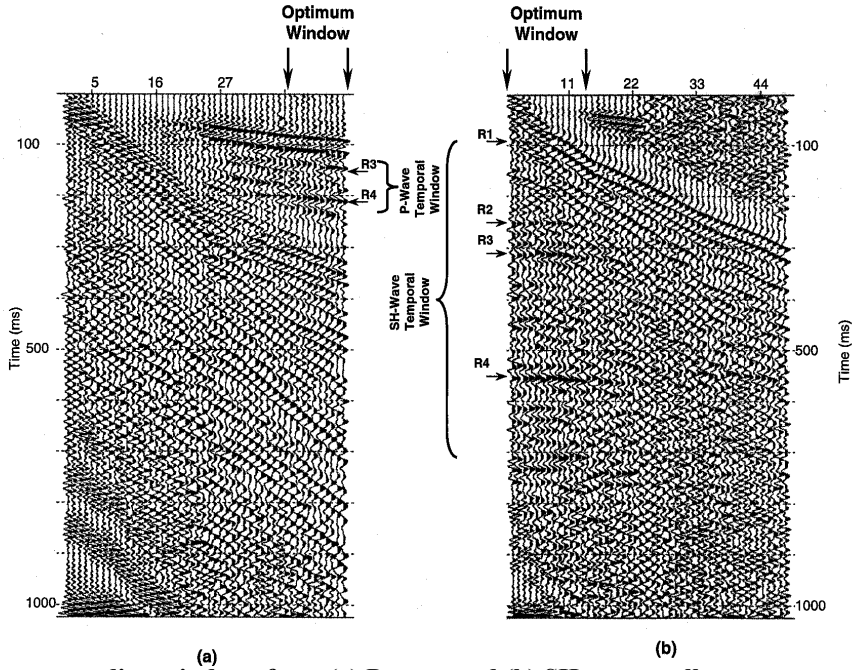


**Figure 5. Optimum recording windows from (a) P-wave and (b) SH-wave walkaway tests at UK-H2.**

The seismic stratigraphy was defined by walkaway soundings (Fig. 5) that were correlated to lithologic changes and cross-hole-derived impedance boundaries identified in a nearby geotechnical borehole (A) (Sykora and Davis, 1993) (Figs. 2 and 4). Sykora and Davis's (1993) visual and laboratory-derived soil characteristics for these units were compared with Olive's (1980) descriptions for final stratigraphic correlation. From this information, we believe that the Paleozoic bedrock (R4) in our study area is overlain by approximately 60 m of the undifferentiated sands and clays (interbedded) of the McNairy-Clayton Formations (R3). The Paleocene Porters Creek Clay, as well as the Eocene silts and clays, appear to be missing in this area. Unconformably separating the McNairy and Clayton Formations from the Pleistocene loess at the surface are nearly 30 m of the predominantly sand and gravel typically associated with the Continental Deposits. This is consistent with stratigraphic investigations performed for the Department of Energy's (DOE) gaseous diffusion facility approximately 1 km east of the study area (Clausen et al., 1992) (Fig. 2). Clausen et al. (1992) reported that most of the Tertiary sediment north of the DOE's southern boundary, in the vicinity of our seismic lines, has been removed by the ancestral Tennessee River. Therefore, the Continental Deposits unconformably overlie the McNairy-Clayton Formations. From the limited information available in the visual and laboratory soil classifications, it is very difficult to reliably distinguish and separate horizons within the Continental Deposits. However, an impedance boundary (R2) does manifest in our profiles at an elevation consistent with that separating a gravel and sand unit from overlying sandy clay and clay units in borehole A (Figs. 4 and 5). The description of the former is consistent with the Mounds Gravel; therefore, this reflector may represent the boundary between the Mounds Gravel and the Late Miocene–Early Pleistocene sand, silt, and clay unit that Nelson et al. (1999) named the Metropolis Formation. Supporting proprietary data suggest that borehole A penetrates a graben that would likely have protected this material from erosion. This environment is similar to that found by Nelson et al. (1999) for the unit. However, without further information, this assessment remains speculative.

An impedance boundary (R1) was also interpreted on line UK-H2 at an average depth of 8 m. This horizon correlated well with the shear-wave impedance boundary and material index changes in borehole A. The relatively low-velocity material above this boundary represents the surface deposits and is composed predominantly of silt, similar to that described by Olive (1980) for the loess units; therefore, we interpreted the boundary as separating the loess and Metropolis Formation. This interpretation is based on nontraditional, but credible, independent physical data sets (i.e., sharp changes in the shear-wave velocities and measured geotechnical index properties of the two units). Although the Sykora and Davis (1993) geotechnical data included visual and laboratory grain-size analyses of the samples, we specifically considered their results showing an abrupt change in plasticity index (Blackall, 1952) for our interpretation. Because of a particle's physical and chemical properties, visual identification, as well as grain-size analyses (i.e., hydrometer), can often be misleading in discerning silts and clays. Simply stated, plasticity is a measure of relative change in soil consistency with water content. Clays are very plastic and silts only slightly plastic, whereas sands and gravels are nonplastic (see any elementary soil mechanics text for specific ranges; e.g., Lambe and Whitman, 1969). Therefore, we took advantage of the objective notion that soil plasticity is a more demonstrative indicator of silt content (relative to a field geologist or engineer's visual classification) in our attempt to identify the loess in Sykora and Davis's (1993) geotechnical field and laboratory information. The sharp

velocity contrast (i.e., much lower shear-wave velocity of the overlying sediments) between the two units suggests lithologic change, as well as a potential geologic age difference (Krinitzsky et al., 1993; Kramer, 1996). Although our correlations are reasonable given the level of detail, more stratigraphic study of the near-surface loess material is required in order to differentiate the individual units (i.e., Peoria, Roxana, and Loveland). This additional information will allow us to better resolve neotectonic timing.

An impedance boundary (R1) was also interpreted on line UK-H2 at an average depth of 8 m. This horizon correlated well with the shear-wave impedance boundary and material index changes in borehole A. The relatively low-velocity material above this boundary represents the surface deposits and is composed predominantly of silt, similar to that described by Olive (1980) for the loess units; therefore, we interpreted the boundary as separating the loess and Metropolis Formation. This interpretation is based on nontraditional, but credible, independent physical data sets (i.e., sharp changes in the shear-wave velocities and measured geotechnical index properties of the two units). Although the Sykora and Davis (1993) geotechnical data included visual and laboratory grain-size analyses of the samples, we specifically considered their results showing an abrupt change in plasticity index (Blackall, 1952) for our interpretation. Because of a particle's physical and chemical properties, visual identification, as well as grain-size analyses (i.e., hydrometer), can often be misleading in discerning silts and clays. Simply stated, plasticity is a measure of relative change in soil consistency with water content. Clays are very plastic and silts only slightly plastic, whereas sands and gravels are nonplastic (see any elementary soil mechanics text for specific ranges; e.g., Lambe and Whitman, 1969). Therefore, we took advantage of the objective notion that soil plasticity is a more demonstrative indicator of silt content (relative to a field geologist or engineer's visual classification) in our attempt to identify the loess in Sykora and Davis's (1993) geotechnical field and laboratory information. The sharp velocity contrast (i.e., much lower shear-wave velocity of the overlying sediments) between the two units suggests lithologic change, as well as a potential geologic age difference (Krinitzsky et al., 1993; Kramer, 1996). Although our correlations are reasonable given the level of detail, more stratigraphic study of the near-surface loess material is required in order to differentiate the individual units (i.e., Peoria, Roxana, and Loveland). This additional information will allow us to better resolve neotectonic timing.

### 4.2 Western Study Area

The western (Olmsted) site lies across the Kentucky–Illinois state boundary, on the lower Ohio River, approximately 26.6 km upstream of its confluence with the Mississippi River. The site is also near the western margin of the juncture of two late Precambrian–Early Paleozoic rifts, the Reelfoot rift and the Rough Creek graben (Figure 1) (Kolata and Nelson, 1991). The Olmsted site is located near the northeastern terminus of the western trend, "Trend 1". In addition, the site is in the near field of the 1984 southern Illinois earthquake swarm (Figure 3). This sequence of almost one hundred earthquakes occurred during the winter of 1984, and lasted for nearly one month. The swarm consisted of predominantly microseismicty; however, a few of the larger events had magnitudes of approximately 3.5 $m_{b,Lg}$ (Ron L. Street, personal communication). Although the earthquakes were recorded instrumentally, a high degree of hypocentral uncertainty exists because of an insufficient number of seismic stations in the region; consequently, any interpretation of epicentral patterns and/or correlation to local structure is highly speculative.

Previous studies have indicated that the Olmsted area, adjacent to the FAFC western boundary, is widely cut by generally northeast-trending faults (Figures 1 and 2) (Ross, 1963; Schwalb, 1969; Davis et al., 1973; Olive, 1980; Kolata et al., 1981). Significant tectonic activity has also been observed west of the study area along the Commerce geophysical lineament in southeast Missouri (Harrison et al., 1999) (Figure 1). Their seismic-reflection and trenching surveys showed extensive late-Quaternary deformation; moreover, these investigations found localized displacement extending into the Holocene sediment. This is the only known location of recent movement outside the central New Madrid seismic zone.

The Paleozoic bedrock in this part of the embayment is generally covered by less than 80 meters of Cretaceous and younger, unlithified sediment (Nelson et al., 1999). Ross (1963) described a general post-Paleozoic stratigraphic succession that consists of upper Cretaceous, Tertiary, and Quaternary sediments; however, boreholes nested for crosshole velocity measurements on the Kentucky shore near the end of our SH-wave reflection profile indicated that Mississippian-aged bedrock is locally overlain by approximately 40 meters of sediment (Fig. 6) (Yule and Sharp, 1988). The corroborating borehole logs in the Kentucky floodplain, immediately adjacent to the river, suggest the Tertiary section has been removed (Yule and Sharp, 1988; Schaefer, 2001). Specifically, the bedrock is unconformably overlain by approximately 20 m of Late-Cretaceous-aged deltaic sediments (i.e., interbedded sands and clays) of the McNairy Formation. Locally, the McNairy also possesses lignite horizons in the lower part of the formation. The remainder of the stratigraphic section above the McNairy Formation consists of undifferentiated Quaternary-aged alluvium (i.e., sands, gravels, and banded silts and silty clays).

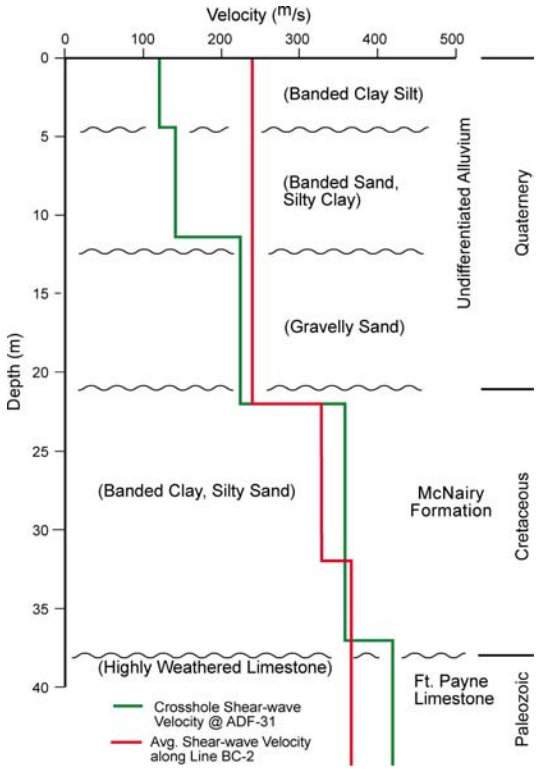


**Figure 6. Local stratigraphy and interpreted velocity model at Borehole ADF-31 (Yule and Sharp, 1988).**

The McNairy Formation is the founding stratum for the Olmsted navigation structure, and as a consequence, the geologic horizon subjected to the most intensive geotechnical tests (Schaefer, 2001). The McNairy sediments consist predominantly of very-fine – fine, dense sands with interbedded layers of stiff clays and silts. In the western study area, the McNairy thickness ranges from a minimum 13 m in the thalwag of the river to a maximum 36 m on the Illinois bank. The sands were classified according the Unified Soil Classification System as SP (i.e., poorly graded sand). The clays and silts are CL and ML (i.e., lean or low-plasticity clays and silts), respectively. The sands are very uniform throughout the formation, with grain sizes predominately ranging between 0.06 mm and 0.3 mm with a mean value of 0.15 mm. Overconsolidation ratios (OCR), a parameter necessary for understanding the vertical stress history of a sediment/soil (Mayne and Kulhawy, 1982; Kulhawy et al., 1989a, 1989b; Mayne and Kulhaway, 1990) were determined from consolidation tests on clay samples taken from various depths within the McNairy Formation. An OCR assesses which of three conditions exist in the field: (1) an OCR ≈ 1 (±20%) indicates a vertical effective stress field that has never been higher than the current magnitude, (2) an OCR > 1 indicates the vertical stress field was once higher than its current magnitude (i.e., erosion, glacial unloading, etc.), and (3) an OCR < 1 indicates a sediment undergoing consolidation from a prior applied load (i.e., not relevant in this environment). The averaged test results from the McNairy Formation yielded an OCR of approximately 2.0; moreover, the OCR showed little variation with depth (Figure 7). Geomechanical index tests were also performed on the samples to assist in comprehensive effective stress calculations. Results showed the specific gravity of the sand is between 2.64 and 2.68, with a void ratio (determined from "undisturbed" samples) ranging from 0.74 to 0.91. The average drained friction angle ($\Phi'$) of the sand was 31˚. In the clay layers, peak values of $\Phi'$ vary from 19 to 22 degrees with residual values as low as 10˚. The average saturated unit weight of the soil is 1,920 kg/m$^3$ (120 lb/ft$^3$). The N-values derived from the Standard Penetration Test ranged from 40 to over 100 blows per foot. The groundwater within the McNairy sands is locally pressurized with heads up to 3 m above the river surface (Schaefer, 2001).

*4.2.1. Geotechnical Stress Indicators ($K_o$)*

The excessive depth to bedrock at the Olmsted site necessitated the design of a pile-supported foundation in the unlithified sediment; therefore, geotechnical tests were primarily performed to evaluate the bearing capacity of the navigation structure's pile foundation. The presence of anomalous in-situ stress was first discovered based on the results of full-scale pile-load tests (i.e., shaft resistance for a low-displacement pile is a function of the effective horizontal stress acting on the side of the pile) and later corroborated by direct measurement using self-boring pressuremeter tests (Schaefer, 2001).

Indirect measurement of lateral stress is a difficult task that utilizes empirical relationships. Also, characterization of in-situ stress conditions is traditionally discussed in terms of the coefficient of lateral earth pressure at rest ($K_o$). Specifically, $K_o$ is the ratio of the effective horizontal stress ($\sigma'_h$) to the effective vertical stress ($\sigma'_v$); the definition also assumes unyielding (i.e., rigid) conditions (Coduto, 1999). Mayne and Kulhawy (1982) empirically suggested $K_o$ for overconsolidated soil defined: $K_o = (1 - sin\Phi')$. However, $K_o$ is complex and dependent on many factors (i.e., effective angle of shearing resistance, shape and interlocking of soil particles,

modulus of elasticity, OCR, elastic and sliding strains, dilation, amount of fines, porosity, densification, crushing, and applied stress), and the use of simple correlations can sometimes lead to significant errors (Hanna and Ghaly, 1992). Consequently, direct (i.e., pressuremeter) and indirect (i.e., pile-load tests) techniques are presented to support the presence of anomalous local stress.

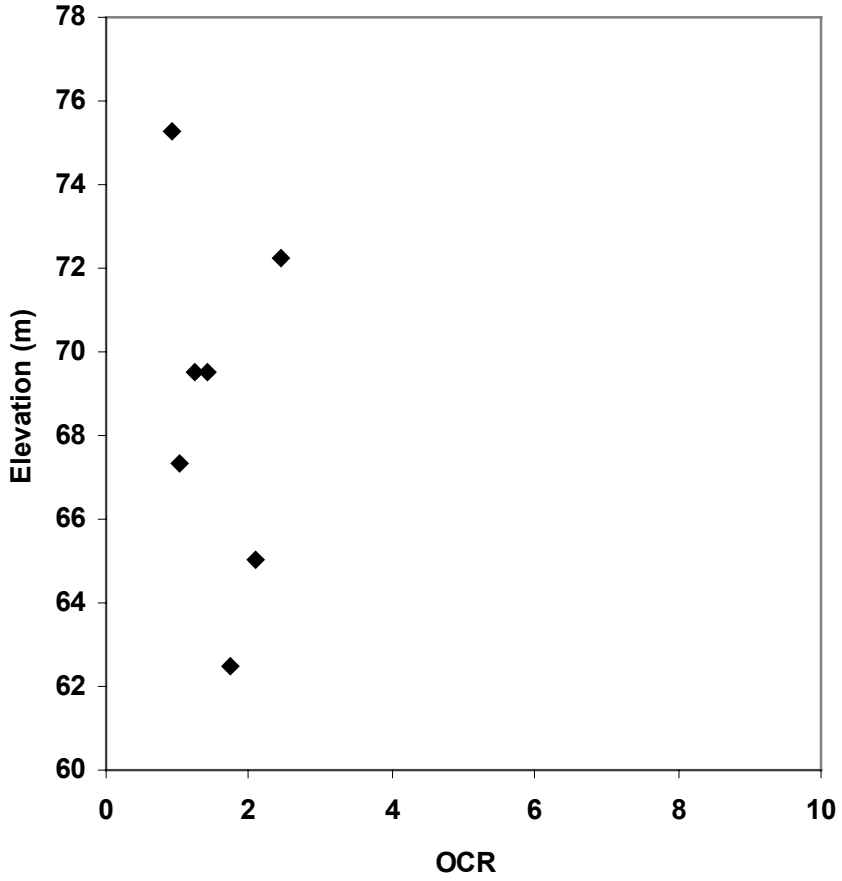


**Figure 7. Overconsolidation ratios profile with depth. These measurements are the result of consolidation tests performed on "undisturbed" samples taken from the McNairy Formation.**

*4.2.1.1 $K_o$ from Pile-Load Tests*

Full-scale pile-load tests were used to backcalculate in-situ horizontal stress in terms of $K_o$. The backcalculation requires characterization of: the pile capacity, soil load transfer (skin friction), skin-friction distribution, soil–pile-interface friction angle (δ), and vertical effective stress profile. H-piles, unlike pipe piles, are low-displacement piles. Moreover, "plugging" was not observed during emplacement; therefore installation effects were assumed negligible.

*4.2.1.2 Pile Capacity*

Six pile-load tests were performed inside a cofferdam on Type 14x117 H-piles that were driven to a depth of 12.2 m (40 ft.). The piles were driven approximately 1.5 m (5 ft.) through the Quaternary alluvial sand and 10.7 m (35 ft.) into the Late-Cretaceous-aged McNairy formation. The average capacity determined from these tests was at least 5000 kN (1124 kips). Four of the tests were taken to the limit of the testing frame 5338 kN (1200 kips) without reaching failure. Specific details of the test setup and procedures were given in Schaefer (2001).

*4.2.1.3 Load Transfer and Shape*

The load transferred to the soil (friction) was evaluated in situ with pile's having both single and multiple strain gauges. The multi-gauge method had strain indicators attached at the pile's tip and midpoint to measure the average compression during the test. The average pile-load length in compression was calculated by:

$$P_{avg} = \frac{A \times E \times \Delta L}{L}$$

where:

$P_{avg}$ = average load in the pile over the length in compression
A = cross-sectional area of the pile
$\Delta L$ = compression of the pile
E = Young's Modulus of the pile
L = length of the pile segment in compression

The results indicated an average load capacity of 4390 kN (986 kips). Other piles were tested with one strain gauge. In this case, a procedure developed by Leonards and Lovell (1979) and reported by Schaefer (2001) was used to estimate the load transfer. The average value of skin friction calculated for these piles was 3880 kN (873 kips). In addition to the compression tests, six tension tests were performed at the site. All of the tension test piles were loaded to 2224 kN (500 kips) (the capacity of the testing frame) without reaching failure. The estimation of horizontal stress from the tension tests was considered a lower bound because the capacity derived in a tension test is all developed in skin friction, thus the actual tension capacity is greater than the maximum load applied in the test. The analyses also indicated that the distribution of skin friction resistance within the McNairy formation was approximately uniform with depth (Schaefer, 2001).

*4.2.1.4 Angle of Internal Friction*

The angle of interface friction between the pile and the soil ($\delta$) typically ranges between 0.66 and 0.75 of the value of the soil's angle of internal friction ($\Phi$) (Leonards and Lovell, 1979). Laboratory shear tests of the McNairy sediments indicated an average $\Phi$ of 31º; consequently, $\delta$ = 25º was selected for analysis. An absolute value of interface friction would be difficult to determine because sand particles were rearranged and crushed during pile installation and loading. Sensitivity analysis using the range of $\delta$ values suggests that the overall effect on $K_o$ in this case is negligible, however.

*4.2.1.5 Vertical and Horizontal Effective Stress*

The vertical effective stress profile was calculated at each test location by multiplying the depth by the saturated unit weight of the soil, then subtracting the pore pressure measured by nearby piezometers. For a uniform distribution of skin friction resistance, the horizontal stress was determined by:

$$\sigma'_h = \frac{F_s}{\tan\delta \times A_s}$$

where:

$\sigma'_h$ = magnitude of effective horizontal stress
$F_s$ = resistance due to skin friction per unit length of pile
$\delta$ = angle of friction between soil and pile
$A_s$ = surface area of pile per unit length.

The surface area for an H-pile was determined assuming that the pile acts as a rectangular shape rather than an "H." The piles were divided into vertical elements based on stratigraphy, and the calculation was applied to each segment. The upper alluvial sand layer was modeled to have a linearly increasing skin friction distribution, whereas the McNairy was modeled to have a uniform distribution. The values of unit skin resistance were adjusted until the total skin friction resistance matched that determined by the Leonards and Lovell (1979) analysis. After the effective horizontal stress was determined, the ratio of effective horizontal stress to effective vertical stress ($\sigma'_h / \sigma'_v$) was calculated. A plot of the effective stress ratio ($K_o$) versus elevation for each of the compression tests is shown in Figure 8. In addition, $K_o$ determined from a typical tension test is shown as a lower boundary. $K_o$ determined by this method may be slightly greater than the initial in situ effective stress ratio, because of the effects of driving and loading of the pile. Nonetheless, the resulting magnitudes of $K_o$ required to develop the static capacities measured in the pile-load tests are quite large.

*4.2.2 $K_o$ from Pressuremeter Testing*

Direct borehole measurements of in situ stress were made with a self-boring pressuremeter (SBPM) following the procedures suggested by Benoit (1995) and Benoit et al. (1995). The individual sample points measured the movement of an expanding membrane with three sets of strain arms oriented 120º apart. The tests were performed in three borings located outside the influence of the pile driving (i.e., 305 m from the cofferdam) (Fig. 3); consequently, the sediments are assumed to be undisturbed. The individual test points were made by advancing the SBPM to the specified elevation (allowing sufficient time for pore pressure to dissipate) and pressurizing the membrane to record total pressure versus cavity strain measured. The orientation of the strain arms could not be determined; thus, identification of the predominant stress orientation was not possible. Future shear-wave birefringence field experiments are planned to assess orientation.

The pressure at which the membrane lifted off the borehole wall (i.e., sediment deformation) was equal to the in situ horizontal stress. The effective horizontal stress ($\sigma'_h$) was subsequently determined by subtracting the pore pressure from the average total horizontal stress measured by the set of strain arms. A value of $K_o$ for each elevation test point was determined by dividing $\sigma'_h$ by the calculated $\sigma'_{v.}$ Figure 9 shows an averaged composite plot of $K_o$ versus elevation determined from the SBPM, along with $K_o$ derived from the compressive pile load tests. The $K_o$ curve is similar to the curves derived from the pile-load tests; however, the magnitude of $K_o$ determined from the SBPM is slightly less at depth. The difference is likely because of the slight increases in lateral stress generated during the pile installation and loading, or possible stress relief caused by soil disturbance during the pressuremeter's advancement in the very stiff deeper sediments.

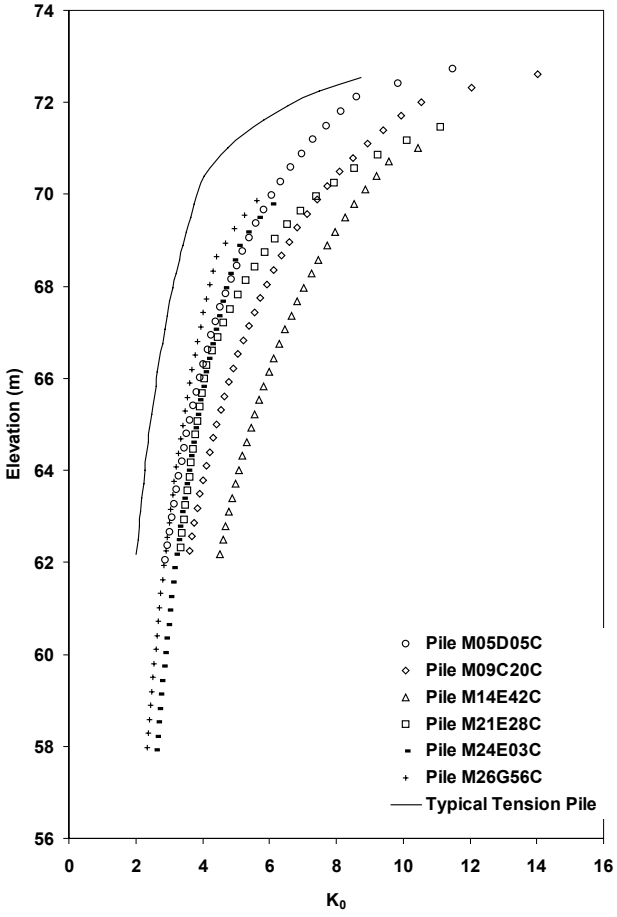


**Figure 8. $K_o$ values backcalculated from pile-load tests. The dashed lines are results from individual piles. The solid line represents a lower bound from the pile tension tests.**

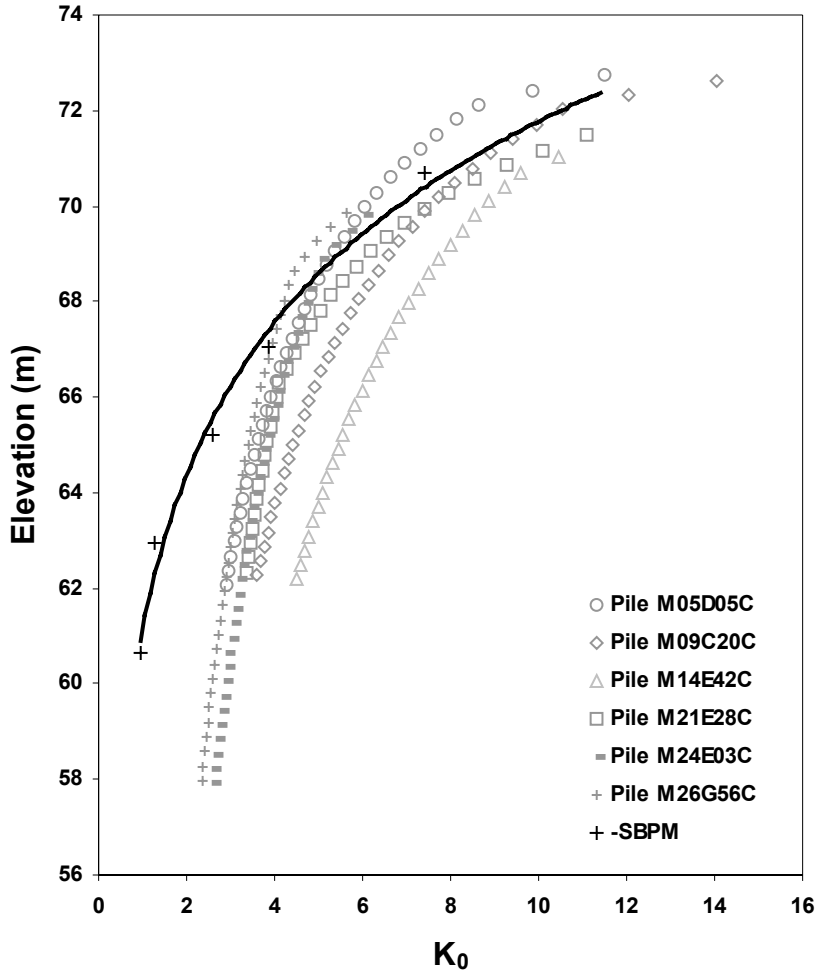


**Figure 9. $K_o$ values derived from pressuremeter tests relative to those back-calculated from pile-load tests.**

## 5.0 DATA ACQUISITION AND PROCESSING

### 5.1 Seismic Reflection

Traditionally, P-wave (compressional wave) seismic-reflection methods have been used to image the neotectonic deformation that propagates into the unconsolidated, water-saturated fill of the upper Mississippi Embayment (Sexton and Jones, 1986; Schweig et al., 1992; Williams et al., 1995; Odum et al., 1998; Stephenson et al., 1999). Common-depth-point (CDP) reflection surveys using the horizontally polarized shear-wave (SH) mode (Woolery et al., 1993, 1996; Harris, 1996; Harris et al., 1998), however, have been found to be more amenable for imaging neotectonic features in near-surface sediment (< 100 m). We believe that shear waves are superior for near-surface imaging because they are "framework waves" (i.e., not affected by the degree of water saturation), and therefore sample the geologic medium more accurately than the fluid-sensitive P-wave. The choice of SH as the preferred phase is based on the idea that SH signals are easy to identify, unlike SV (vertically polarized shear wave) signals, because of the lack of mode conversion at the refracting and reflecting boundaries. The lower velocity S-mode also shifts the optimal acquisition window to the nearer offset, as well as providing expansion of

the spatial and temporal optimal window (Fig. 5). The increased temporal window permits easier, more accurate identification of the reflecting boundaries as a result of the increased separation of the signal and coherent noise events. The broader spatial window at the near offset permits application of increased fold without introducing adverse wide-angle reflection effects. In addition, our experience shows that although S-waves commonly have frequencies only one-half to one-third that of P-waves, the P-waves have velocities five to 10 times higher than S-waves. Consequently, we estimate that resolution can be improved by a factor of 2 to 3 through the use of S-waves. This is a very important point when considering small fault displacements (i.e., 2 to 3 m). For example, UK-H2 in the eastern study area has a measured 50 Hz dominant frequency and a 150 to 500 m/s velocity range. This yields a temporal resolvable limit (i.e., calculated by the one-quarter wavelength criteria of Sheriff and Geldart, 1989) ranging between 0.75 m in the very near surface to 2.2 m at the top of bedrock. The detectable limits are considerably smaller (i.e., 1/10 $\lambda$ to 1/20 $\lambda$). The spatial resolution of R1 to R4 is constrained between approximately two and four shotpoints based on the radius of the first Fresnel zone.

Reflection data from all sites were collected in P- and SH-mode with a 48-channel engineering seismograph. Surveys were shot off-end with an active spread of twenty-four or forty-eight geophones. P-wave data were collected with 40 Hz vertical receivers, and the SH-wave lines were collected with 30 Hz geophones oriented perpendicular to the seismic line. The group and shotpoint intervals were typically between 2 and 4 m. The seismic energy was generated by five to 10 impacts of a 4.5 kg hammer on a small aluminum plate. The SH-wave energy was generated with a similar number of horizontal blows to a 12 kg modified H-pile section oriented perpendicular to the spread. To ensure the initial accurate identification of SH events, impacts were recorded on each side of the energy source for the walkaway tests; however, impacts were only recorded on one side during general production because of the good data quality. In an attempt to generate higher frequencies, the energy source used for the latter SH lines was a smaller 1.8 kg engineer's hammer and 6 kg H-pile section. Generally, nine impacts were applied at each shot location. Seismograph acquisition parameters for lined typically included filter settings of 25 Hz (lowcut) and 250 Hz (highcut), and a 1 second record length. The sampling interval was 0.5 ms. A 60 Hz notch filter was used near electrical power sources.

All seismic data were processed on a personal computer using the commercial signal-processing software VISTA 7.0. The processing sequence applied to the shallow CDP reflection data is shown in Table 1. Coherent noise muting, digital filtering, trace editing, appropriate trace balancing, and careful correlation statics were the primary processes in improving the pre-stack quality of the events seen on the raw field file. This is an acceptable, routine processing sequence for most high-resolution, shallow (< 100 m) seismic-reflection work (Steeples and Miller, 1990; Baker, 1999). These standard near-surface data-processing procedures are similar to those used in the petroleum industry, but scaled down and conservatively applied. Other, nontraditional shallow-reflection processing methods such as f-k filtering, deconvolution, and migration were considered, but because some degree of resolution degradation occurs with the application of any processing step, significant improvement in the signal quality had to be demonstrated before such applications were justified. Instances where data quality from an f-k filter was found to warrant the application, the filter slopes were very gentle in order to minimize artifact generation and the “wormy” appearance of a more severe application. Deconvolution is

also often considered a nontraditional procedure in shallow reflection work. The process has basic assumptions (i.e., random reflectivity series, high signal-to-noise ratio data) that are often violated by the shallow data sets (Baker, 1999). Although the datasets often appeared to have a sufficient number of reflectors with a relatively high signal-to-noise ratio for constructing an operator, the resulting section appearance was somewhat "smeared"; consequently, the process was judged to be detrimental to overall resolution. Therefore, deconvolution was not applied to the any of the final sections. Another frequently abused shallow processing procedure is migration. The migration of data with shallow reflector depths and relatively low velocities, particularly in shear-wave exploration, often provides insignificant image improvement. One reason for this is that a shallow reflector's energy is already concentrated at the diffractor's apex, and migration simply doesn't make a significant difference (Black et al., 1994). In addition, as noted by Black et al. (1994), the diffraction tails often have amplitudes lower than the background noise, and the migration procedure can cause an overall lowering of the data coherency. Migration was not applied to our lines because the procedure did not improve the image quality (i.e., again producing a "smearing" effect) or change any interpretation; therefore, the degradation of resolution could not be justified. After preliminary processing, we also concluded that higher fold stacks were adversely affected by lateral discontinuities and wide-angle frequency distortions (including NMO stretch); consequently, a 12-trace window was selected for all lines (see optimum windows in Figs. 10 and 11) that produced six-fold stacked sections and maintained optimal data coherency.

**Table 1.**

| Processing Steps |
|---|
| 1. **Reformat** |
| 2. **Spherical Divergence Gain** |
| 3. **Elevation Statics** |
| 4. **Bandpass Filter** |
| 5. **Sort to CDP Gathers** |
| 6. **Velocity Analysis** |
| 7. **First-Break and Surgical Muting** |
| 8. **Normal Moveout Corrections** |
| 9. **Surface Consistent Statics (10 ms max. shift)** |
| 10. **CDP Stack** |
| 11. **Automatic Gain Control** |
| 12. **f-k Filtering** |

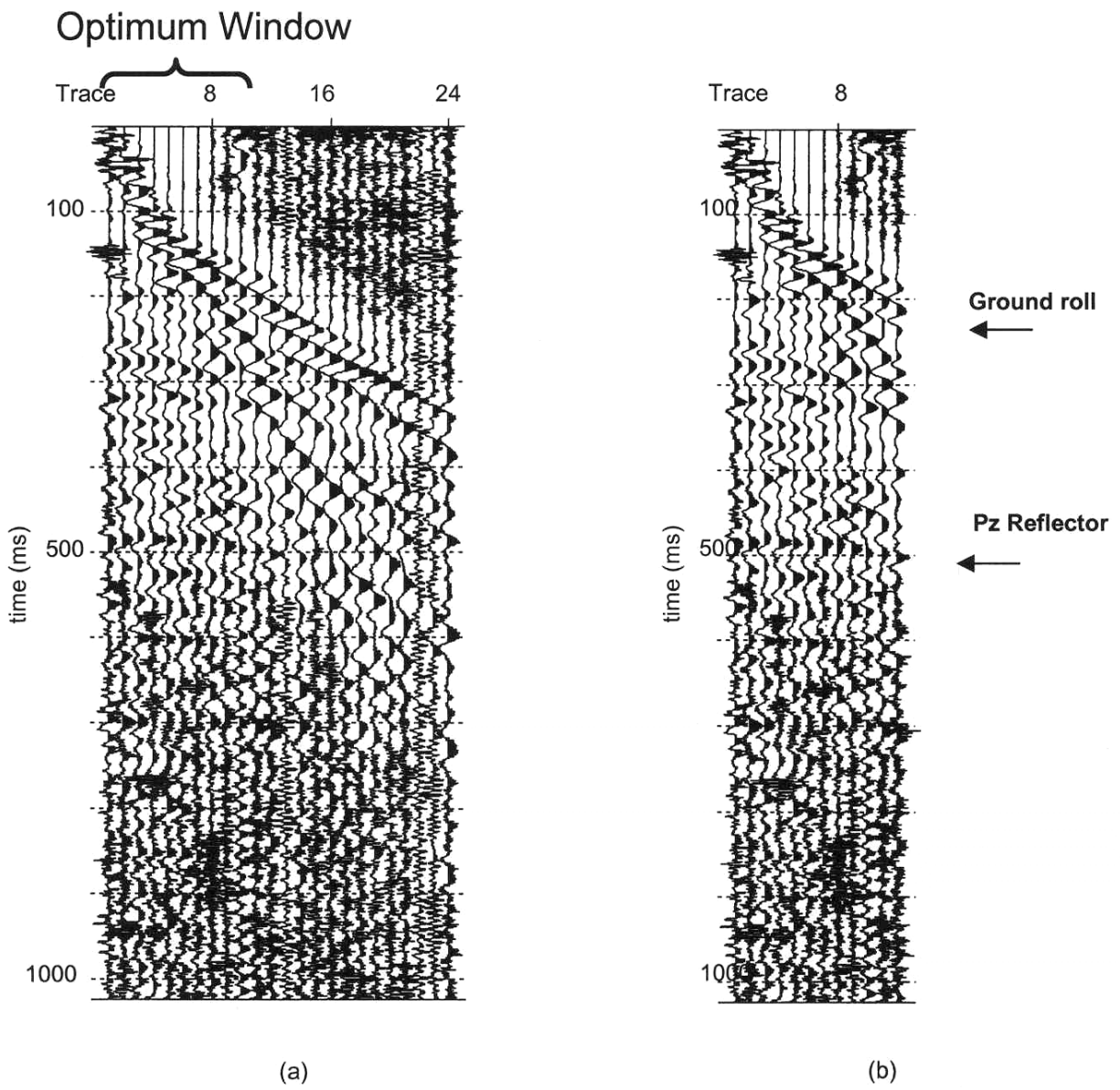


**Figure 10. A typical example of a raw field file from the eastern study area (UK-B3). The first 12 channels were selected as the optimum window.**

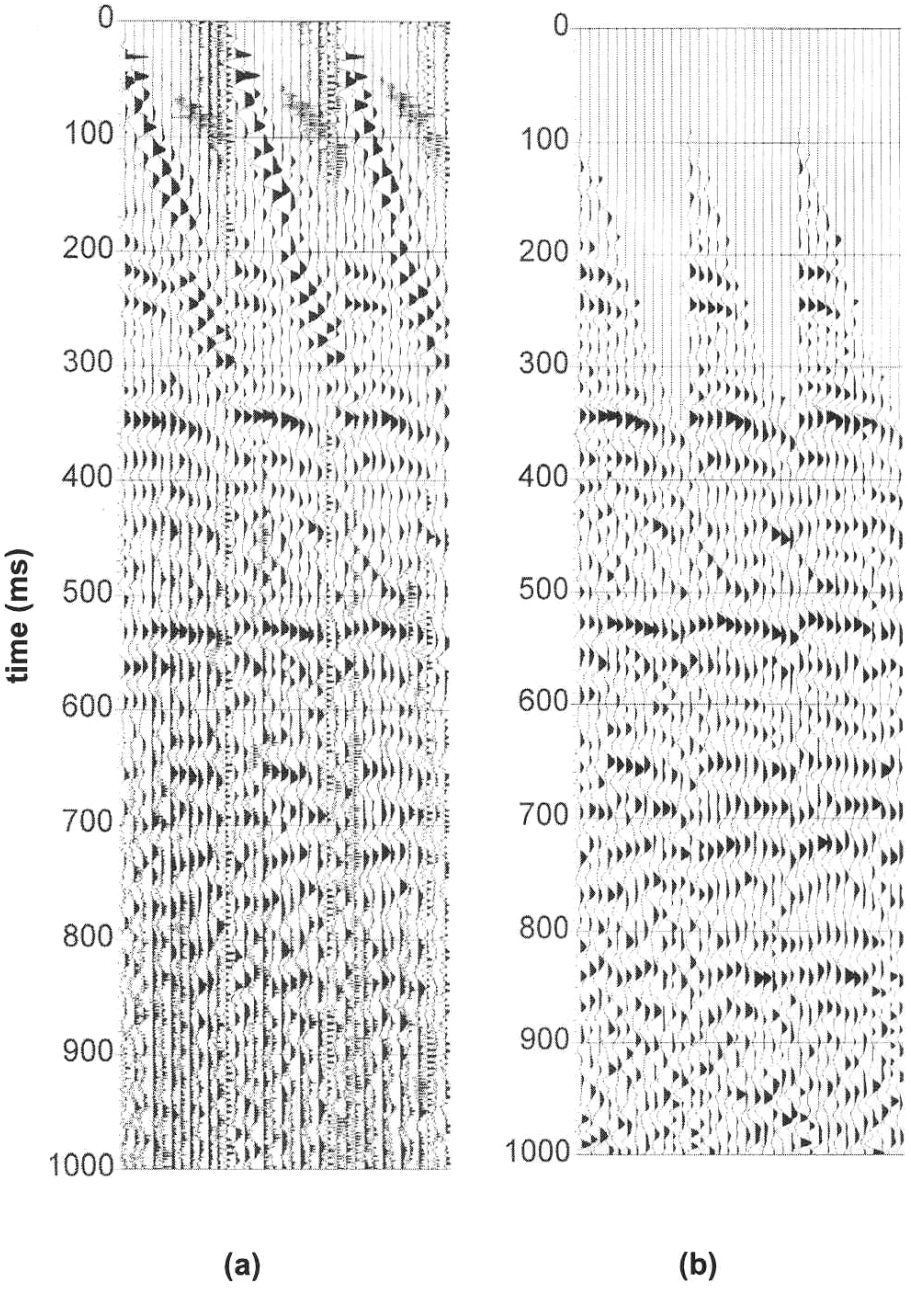


**Figure 11. Typical example of a raw (a) and processed (b) field files from the western study area (UK-BC2).**

## 5.2 Ground-Penetrating Radar

The GPR data were acquired with a Sensors and Software PulseEkko 100 system. The field trials showed that the large amount of fines present in the soils of the eastern study area severely attenuated the signal; however fewer fines present in the alluvial sediments in the western study area allowed penetrations depths down to approximately 5 meters. Field trials identified the 50 MHz bi-static antennae with 1-m separation and a 0.5-m group sample interval as the optimal configuration for data quality and field efficiency. The near-surface silty sands and gravels in the western study area have an estimated velocity of 0.1 nanoseconds per meter. The final profiles were DEWOWED and gained.

# 6.0 DATA OBSERVATIONS

## 6.1 Eastern Study Area

*6.1.1 Seismic Profile UK-B3*. The 710-m-long west-northwest–east-southeast-oriented profile is a segment from Langston et al.'s (1998) previously unpublished 4.6 km line. The data was acquired along a paved highway, and was part of the general area reconnaissance. The data quality is fair, and is representative of the entire line. Three reflecting horizons (R2, R3, and R4) are identified in the section (Fig. 12a–b). The most prominent reflector is R4, interpreted as the top of the Paleozoic bedrock (Pz), at approximately 500 ms (Fig. 10). Although reasonably coherent, the horizon appears highly disrupted along the profile length as evidenced by the numerous diffraction patterns. The R3 (~300 ms) and R2 (~200 ms) reflectors are interpreted as the top of the McNairy and Mounds Gravel formations, respectively, but both appear weak and discontinuous throughout most of the profile. Geologic structure in near-surface seismic-reflection profiles is interpreted from noticeable vertical and horizontal reflection discontinuities, as well as the diffracted wave patterns. These criteria indicate clear geologic structure (Fig. 5a–b) between CDP numbers 125 and 200. The interpreted fault zone, comprised of six fault strands, has an apparent throw down to the southeast. The measured displacement across the R4 horizon is nearly 30 m. Most of the displacement occurs on the northwestern-most south-dipping fault strand. This suggests a predominant normal slip for this fault; however, four of the six faults in the zone dip to the NW, and most of the SE-down throw on the R3 reflector occurs across two of these NW-trending strands. The deformation area also broadens in the nearer surface. These observations support an overall reverse motion across the fault zone in post-R3 (Cretaceous) time. Although it is evident that the disruptions have crossed the Pliocene–Pleistocene horizon (Mounds Gravel), the data are not sufficiently clear to reasonably estimate displacement magnitude. In addition, these data give no clear indication as to the presence, or magnitude, of a strike-slip component.

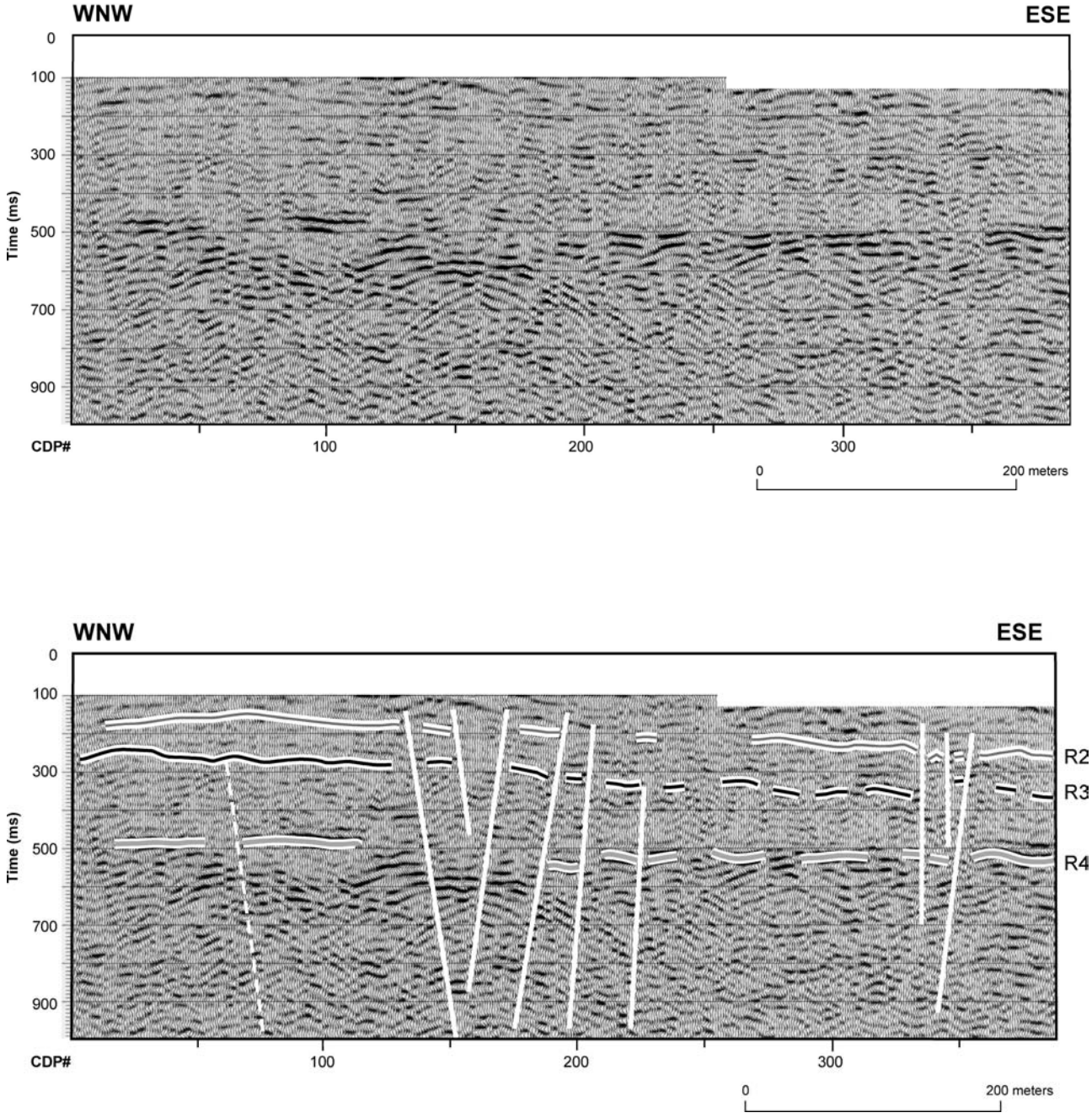


**Figure 12. (a) Uninterpreted and (b) interpreted stacked SH-wave reflection profiles from UK-B3.**

A second area of deformation is interpreted at CDP number 340. The relatively strong R4 reflector exhibits downthrow to the northwest; however, offset reversal is evident along the R3 and R2 horizons. The displacement is approximately one-half that measured between CDP numbers 125 and 200. Again, the data quality does not allow for a confident displacement estimate in the nearer surface. Other structures may be interpreted along the R4 horizon, but are not discussed because it is unclear that they affect the entire time section.

*6.1.2 Seismic Profile UK-H2*. The 400 m profile is part of a 1.2 km northeast–southwest-oriented line sited to intersect structure seen in proprietary lines to the northeast (Fig. 2). A decreased sampling interval, as well as tighter acquisition geometry and a more compact energy source (higher frequency energy generation), were adopted to enhance the images of the Quaternary horizons compared to previously acquired reconnaissance lines. The profile was also collected along a paved highway, and special attention was given to the source-to-ground energy coupling. The resulting data quality is considered excellent for this area (Fig. 13a–b). Four reflection horizons (R1, R2, R3, and R4) that closely correlate to the material changes identified in the Borehole A data are shown on the section. The most prominent reflector (R4) was interpreted as the top of the Pz bedrock at approximately 500 ms; the horizon is continuous and coherent throughout most of the section. In addition, the R3, R2, and R1 horizons are observable at approximately 300 ms, 200 ms, and 75 ms, respectively. These shallow reflection horizons were interpreted as the top of the McNairy-Clayton, the top of the Mounds Gravel, and the base of the loess deposits (top of Metropolis Formation), respectively. All horizons are relatively strong and coherent throughout most of the profile. Two faulted areas are interpreted between CDP numbers 100 and 200 (Fig. 7b). The more prominent is centered near CDP number 175, and has a relative throw along the R4 (Pz) reflector down to the southwest. The total measured displacement across this horizon is nearly 35 m. Moreover, the discontinuity appears to propagate through the entire time section. Measured offsets of 18 m and 4 m affect the Cretaceous-aged R3 (K) and Pleistocene R1 (QPt) horizons, respectively. The predominant character is normal slip displacement across the Pz reflector. However, slight offset reversals in the apparent throw along the R3 horizon and above, emphasize the episodic nature of these features. An oblique intersection angle of the seismic line and the fault planes may obscure the actual displacement, and exaggerate the width of the overall structure. The presence of a broad flexure and lack of sharp displacement is also consistent with a later SW-up displacement, exactly reversing an initial SW-down displacement.

In addition to the structural relief, a seismically opaque, or “washed-out” zone appearing between CDP numbers 300 and 360 is also indicative of intense deformation. This anomalous zone, bounded by relatively strong, coherent reflectors, appears across the entire time section. Although the bounding reflections do not exhibit a definitive displacement, the presence of diffractions and the broken, uneven character of the weak R1 horizon suggest structural deformation. Again, the presence of a strike-slip component is indeterminate.

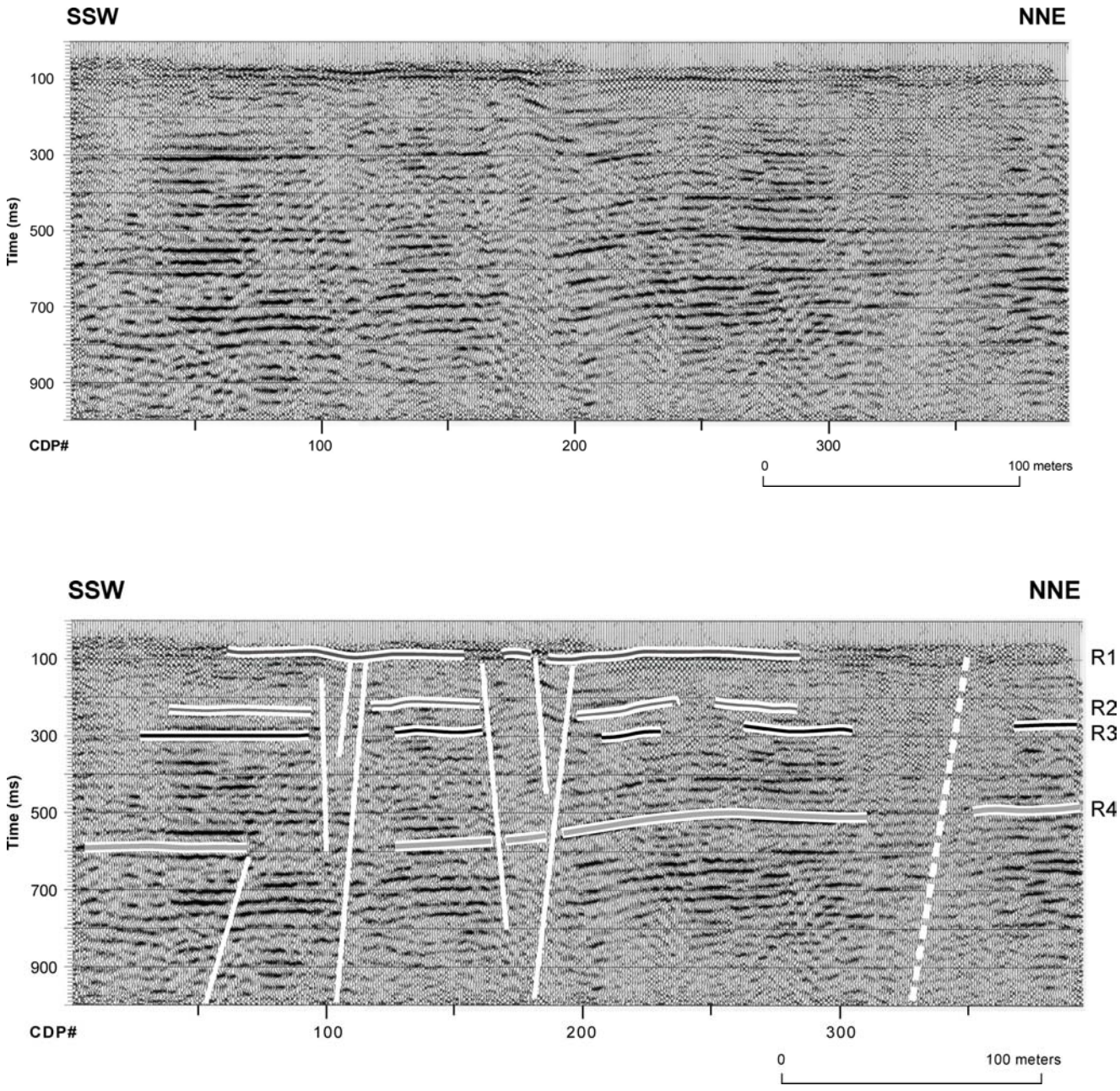


**Figure 13. (a) Uninterpreted and (b) interpreted stacked SH-wave reflection profiles from UK-H2.**

## 6.2 Western Study Area

*6.2.1 Seismic Profile UK-BC2*. The six-fold, 0.75 km profile (BC-2) shown in Figure 14a–b is part of a 1.8 km northeast–southwest-oriented survey sited to intersect structure interpreted from previous drill holes and refraction soundings at the Olmsted site (Yule and Sharp, 1988; Schaefer, 2001). The data were acquired along a graveled access road, and special attention was given to the source-to-ground energy couple (Figure 3). The resultant data quality is considered excellent for these high- attenuation sediments. Four reflection horizons (R1, R2, R3, and R4) were observed along BC-2. These horizons closely correlate to the material changes identified in the nearby borehole ADC-31 (Figures 3 and 6). The most prominent reflector (R4), at approximately 290 ms (east-northeast end of BC-2), was interpreted as the top of the highly weathered Paleozoic (Pz) bedrock; the horizon is continuous and coherent throughout most of the section. In addition, the R3, R2, and R1 horizons are observable near the east-northeast end of the profile at approximately 250 ms, 200 ms, and 135 ms, respectively. These more shallow reflections correlated to an intra-McNairy unit, the top of the McNairy Formation, and an intra-alluvial horizon, respectively. All horizons are relatively coherent along most of the profile.

The section exhibits indicators of episodic tectonic deformation that extend above the Paleozoic bedrock into the Quaternary alluvium. Fault interpretations were defined by: (1) offset reflectors, (2) abrupt termination of strong reflection signals, (3) diffraction patterns, (4) abrupt change in reflection dips, and (5) associated folds. Using these guidelines, three prominent faulted areas, located near CDP numbers 60, 310, and 375, are interpreted along the profile (Figure 14b). The deformation centered at CDP number 60 (F1) is near vertical, and has a relative throw along the R4 (Pz) reflector down to the west-southwest. The total measured displacement across this horizon is approximately 26 m. Moreover, the discontinuity appears to propagate through the entire time section; measured offsets of approximately 7 m and 6 m affect the top of the McNairy Formation (R3) and intra-alluvial (R1) horizons, respectively. The predominant character is normal displacement across the Pz reflector; however, the slight offset reversal (i.e., apparent throw along the R3 horizon and above) and the onlap character of the McNairy horizon emphasize the episodic nature of this feature. In addition, the presence of an apparent force fold in the hanging wall and a lack of sharp displacement are consistent with a structural inversion (i.e., later southwest-up displacement that reverses the initial southwest-down throw). Note that an oblique intersection angle between the seismic line and the fault planes may exaggerate the width of the overall structure.

A second area of deformation having an overall structural style similar to F1 is centered near CDP number 375 (F2). The interpreted F2 fault plane is also a near-vertical normal-slip displacement with a relative throw along the R4 (Pz) reflector down to the west-southwest. The total measured displacement across this horizon is approximately 21 m, and the discontinuity again extends above the Paleozoic top to at least the Cretaceous-Quaternary unconformity. The offset at this horizon is roughly 5 m, but the relatively poor signal quality at this point makes the accuracy of the measurement suspect. Signal incoherency above the R2 horizon and the apparent flexure in the weak reflection at 100 ms suggests that the deformation may extend into the very near surface (< 10 m); however, this also remains speculative because of the localized

degraded data quality. A slight thickening of the intra-Cretaceous horizon (R2) and the presence of a force fold in the hanging wall are also consistent with a structural inversion similar to F1.

The third area of deformation is centered at CDP number 310 (F3). F3 is indicative of a relatively younger structure with predominantly reverse motion. Unlike the depositional onlap exhibited at F1 and F2, the horizons displaced by F3 show a more symmetric deformational style extending across the bedrock to the top of the McNairy Formation (R3). In addition, the interpreted fault plane is high angle (slight west-southwest dip) with an overall apparent downthrow to the east-northeast. Additional fault strands associated with the primary structure are near vertical and appear antithetic. Although total vertical displacement across the F3 Paleozoic horizon is approximately 20 m, an accurate measurement is difficult because of the nonuniform (folded) geometry of the reflectors in the hanging wall.

*6.2.2 GPR Profile UK-BC2*. The single-fold, 0.45 km profile (BC-2) shown in Figure 15 was collected approximately coincident with UK-BC2 CDP traces 350 to 475. The GPR data interpretation indicates that the deformation characteristics imaged by seismic reflection extend to within 2 to 3 meters of the ground surface; nearby Corps of Engineers interpreted borehole data also suggest that these materials are Holocene-aged deposits.

## 7.0 DISCUSSION AND SUMMARY

### 7.1 Eastern Study Area

Complex geologic structures associated with the Fluorspar Area Fault Complex have been well known for several years; however, Nelson et al. (1997, 1999) have only recently documented episodic tectonic movement along fault complex structures through surface mapping investigations at the northern end of the Mississippi Embayment in southern Illinois. They reported long, narrow, relatively steep grabens bounded by both normal and reverse faults that suggest pull-apart structures produced by strike-slip faults. Nelson et al. (1999) found evidence of widespread neotectonic displacements that extend into the Miocene and early Pleistocene sediment. Their mapping also indicate that faults typically strike N20°E to N40°E and outline narrow grabens.

Large, complex signal anomalies are seen in the marine "sparker" reflection surveys acquired for the U.S. Army Corps of Engineer's construction projects along the lower Ohio River. These anomalies are believed to be low-resolution images of the extension of the fault complex beneath the embayment sediment cover of western Kentucky (Fig. 2) (Alpine Geophysical Associates Inc., 1966). We used these data and strikes interpreted by Nelson et al. (1997, 1999) to site the shallow SH-wave seismic-reflection surveys. The structures imaged by these lines are near the northwestern boundary of the Raum Fault Zone that was described by Nelson et al. (1999). They placed the Raum Fault Zone 2 to 3 km southeast of and parallel to the Lusk Creek Fault Zone (Fig. 2). The Raum Fault Zone widens to nearly 2 km in their southern study area (southern Illinois) and exhibits a change in the net throw down to the southeast. They also reported at least

two episodes of post-Pennsylvanian, pre-Cretaceous movement: reverse faulting that raised the northwest block, followed by normal faulting that lowered the northwest block

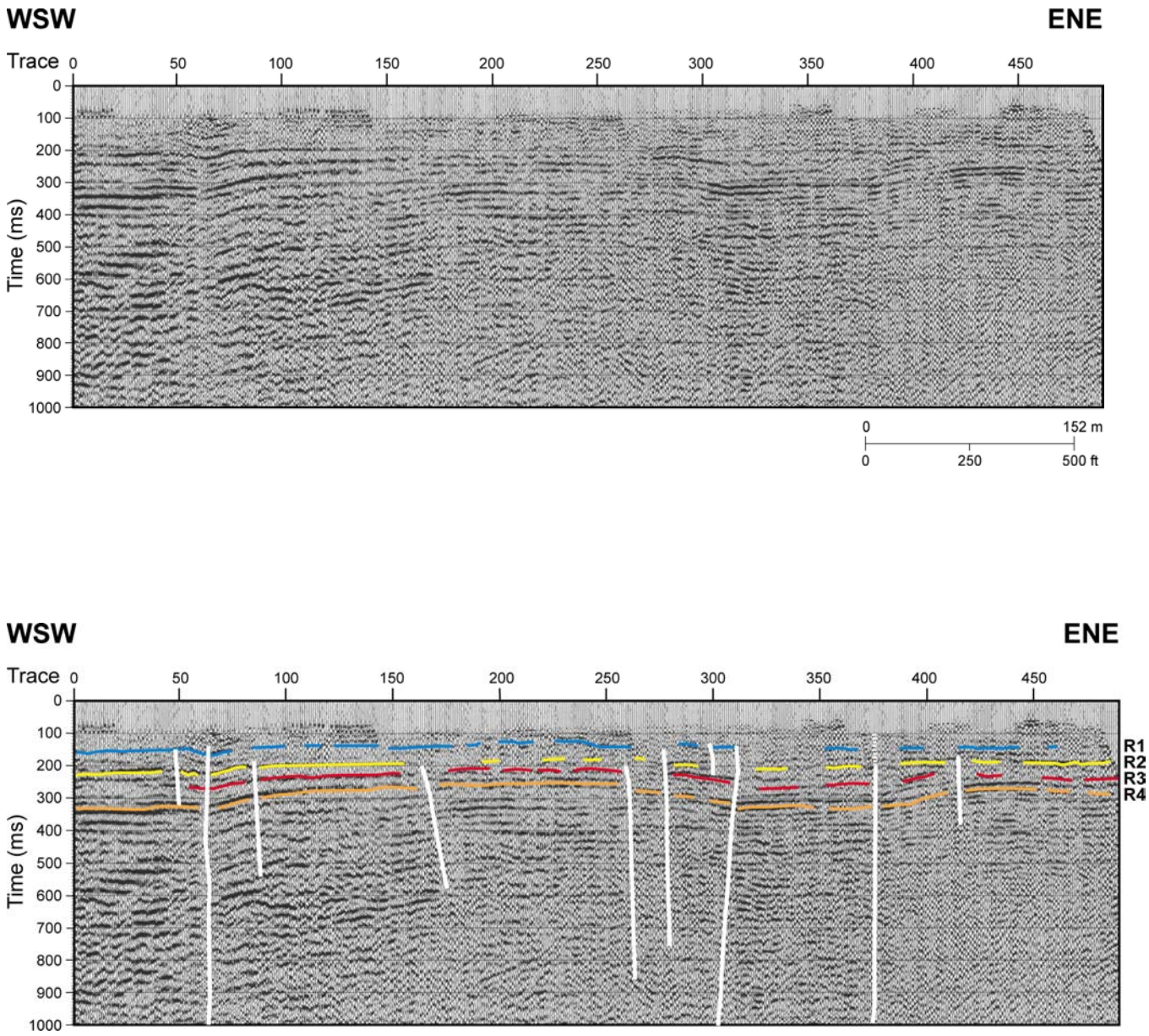


**Figure 14. a) Uninterpreted and b) interpreted SH-wave six-fold stacked image along profile BC-2.**

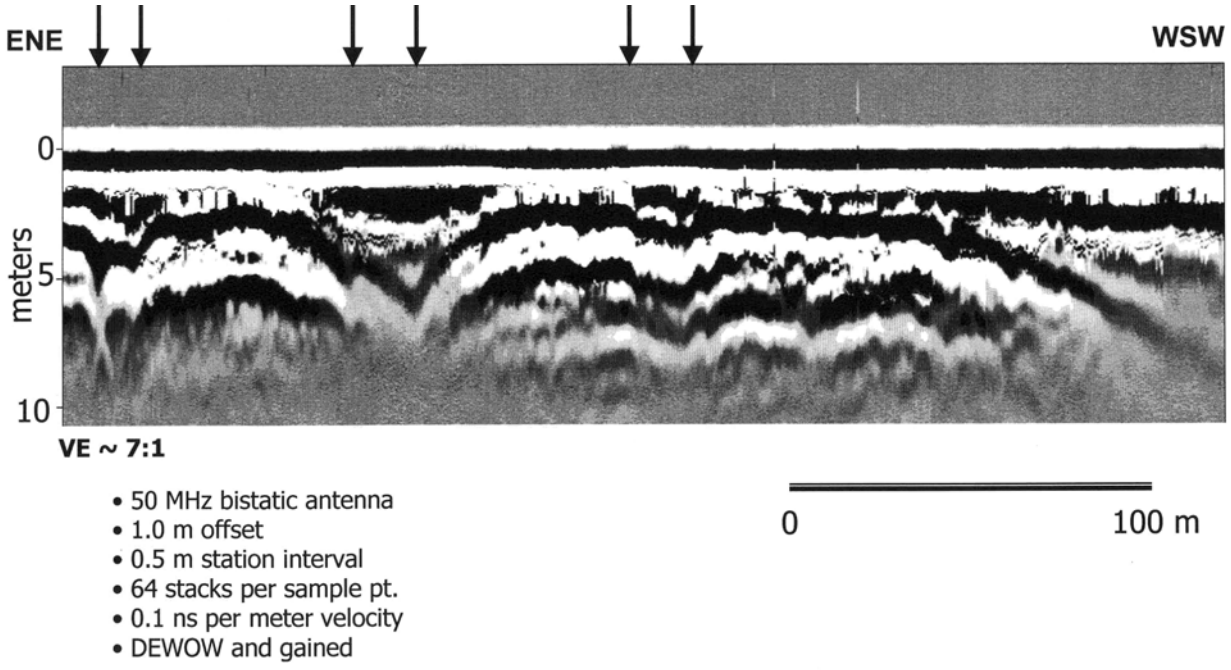


**Figure 15. Ground penetrating radar profile collected between approximately UK-BC2 traces 350 and 475. The arrows indicate interpreted faults within 2 to 3 m of the ground surface.**

although strike-slip motion also may have occurred. These investigations found no Holocene movement, however. Not surprisingly, the "sparker" data are inadequate to resolve detail at this level. Based on the anomalies and the local and regional strike, additional structure associated with the Raum Fault Zone may lie a short distance (1 to 2 km) to the west of our S-wave profiles. Nonetheless, episodic movement can also be seen in the Raum Fault Zone's ancillary structure imaged in this investigation. Differential offset, throw reversal in the post-Cretaceous horizons, as well as a slight local thickening of the R4-R3 and R2-R1 sections in the vicinity of the faults (i.e., UK-H2) provide evidence. The data also show that neotectonic movement has affected the Quaternary section to at least the base of the loess deposits. Whether the displacement is placed at the base or within the loess deposit depends on the correlation accuracy of the assigned near-surface stratigraphy.

Both profiles lack a strong, coherent, and continuous reflection from the ideally sharp bedrock/soil impedance boundary; we believe this indicates an intensely weathered/faulted Paleozoic bedrock surface. Difficult drilling conditions encountered at the sediment-bedrock boundary (Clausen et al., 1992, study) are corroborative evidence. However, the most important fact is that some of the geologic structures identified along this horizon clearly propagate higher into the nonlithified sediment overburden, and if our interpretation is correct, then faulting is present across the Metropolis Formation (i.e., Illinoian) to the base of the loess (Illinoian–Wisconsinan?). This neotectonic activity will have implications for the seismic design loads of critical or high-hazard structures in the area.

Although these SH-wave profiles represent the first high-resolution images of Quaternary Fluorspar Area Fault Complex reactivation in the Mississippi Embayment sediment of western Kentucky, the data are too limited to provide a definitive understanding of the fault kinematics or their potential relationship to Wheeler's (1997) projected New Madrid seismicity. The extent of faults and their potential relationship to through-going Reelfoot Rift structure is critical for delineating the inferred boundary separating the seismically active Reelfoot Rift from the relatively sparse seismicity in the area of the Rough Creek Graben and Fluorspar Area Fault Complex in southern Illinois.

## 7.2 Western Study Area

Indirect (pile-load) and direct (pressuremeter) geotechnical tests indicate the presence of elevated lateral stress conditions (i.e., $2 \leq K_o \leq 12$) in the near-surface, unlithified sediment at the Olmsted project site. Understanding the origin of this stress variance, based solely on these test results, is unclear because of a complex regional geologic history that includes direct tectonic mechanisms, as well as nontectonic or indirect-tectonic phenomena such as transient overburden (e.g., fluvial or glacial deposition and erosion) and dynamic shear loads (e.g., earthquakes), respectively. Past overburden loads are not believed to be the source of the current anomalous lateral stress, because the clay samples obtained from the McNairy Formation would need an unusually high OCR (i.e., 25) to satisfy the measured in situ condition and its relationship to sediment properties, as given by Mayne and Kulhawy (1982). The OCR profile at the site was derived in the laboratory from consolidation tests performed on "undisturbed" McNairy samples; results indicate an average OCR of approximately 2 throughout the entire sediment column (Fig. 7). Consequently, the high lateral stress generation from past vertical loads is not reasonable. Anomalous stress can also be derived from indirect tectonic sources such as permanent strain in the sediment accumulated during past earthquake loads. The alteration in the lateral state of stress in sand from dynamic loading has been documented in controlled tests (Zhu and Clark, 1994). The Zhu and Clark (1994) results indicate that lateral stress in sand can increase or decrease during vibration, depending on the initial state of stress. Specifically, the tests found that an initial $K_o < 1$ resulted in a lateral stress increase, but an initial $K_o > 1$ caused a decrease in overall lateral stress. In both cases, however, the deviator stress tended toward the isotropic stress state of $K_o = 1$. Therefore, the elevated in situ $K_o$ values present at the site suggest that dynamic shaking is also an unlikely source.

Although the geotechnical measurements exhibit clear indications of elevated lateral stress, they are unable to provide a reasonable idea of origin with any degree of certainty. The documentation of local neotectonic geologic structure and the associated deformational style offer insight because of its mesoscale response to local stress conditions. It should be noted that neither the geotechnical tests nor the reflection survey offers a defensible hypothesis for a stress origin independent of the other; however, an integrated assessment of the high earth pressure coincident with neotectonic compressive features does provide sufficient constraints for the source alternatives. The high-resolution SH-wave profile imaged a well-defined horst-graben structure with a complex episodic history; consequently, we propose that the origin of the high lateral stress is directly related to regional tectonics. Sufficient data are unavailable to provide a comprehensive summation of a specific tectonic mechanism (i.e., thermal anomaly, structural

heterogeneity, etc.); however, Figure 16 is a simple schematic diagram suggesting a potential event sequence for the interpreted structure. The most important episode in the sequence is a structural inversion (Tertiary?) that is evidenced by predominant antiformal folds in the R2–R4 hanging wall (horst) reflectors. Small-amplitude force folds may also be present in the Quaternary intra-alluvial horizons, although the data quality of these very near-surface horizons makes this interpretation less definitive.

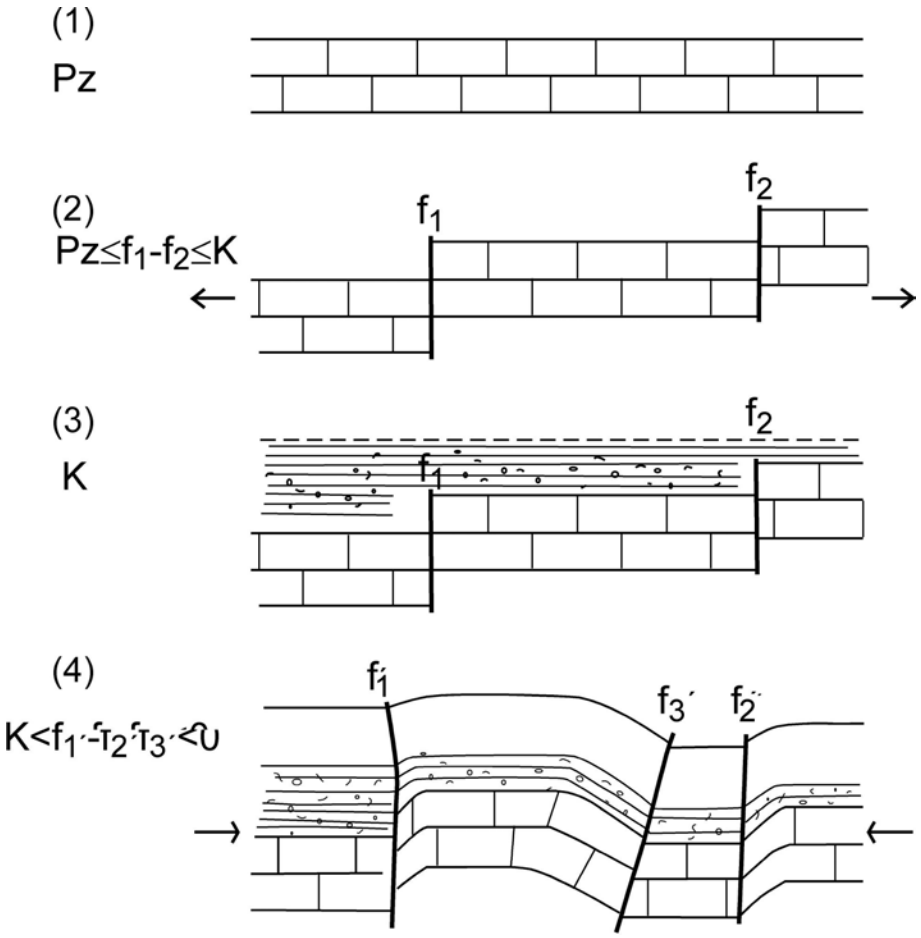


**Figure 16. Simple schematic diagram showing possible tectonic events responsible for interpreted structure imaged in profile BC-2. The "blocked", "stippled", and white patterns represent the Paleozoic, Cretaceous, and Quaternary horizons.**

A direct tectonic origin for the elevated lateral stress discovered in the near-surface unlithified sediment is supported by geophysical images of local neotectonic structure, as well as regional stress patterns, local seismicity, and other regional neotectonic structure. The seismic-reflection profile documented in this study indicated pronounced compressive characteristics in the local geologic structure; however, the latest stratigraphic extent of the stress effects (i.e., all measurements were in the McNairy Formation), as well as a more accurate comparison of stress orientation with the orientation of local structure and regional stress, remains unknown. In order

to better understand these unknowns, acquisition of additional pressuremeter measurements in the Quaternary sediments, as well as surface (see Harris, 1996) and downhole shear-wave birefringence surveys are planned.

## 8.0 JOURNAL PUBLICATIONS AND CONFERENCE PROCEEDINGS

Woolery, E., J. Schaefer, and Z. Wang (2003). Geotechnical and geophysical indicators for local anomalous stress in the unlithified sediment of the northern Mississippi Embayment, central United States. *Tectonophysics* v.368, p. 139 – 153.

Woolery, E., J. Schaefer, and Z. Wang (2002). SH-Wave Seismic-Reflection Evidence for a Tectonic Origin of Anomalous Stress in Near-Surface Unlithified Sediment, Midcontinent, United States. *Eos Trans. AGU, 83*(47), Fall Meet. Suppl., Abstract T22B-1155

Woolery, E., and R. Street (2002). Quaternary fault reactivation in the Fluorspar Area fault complex of western Kentucky–Evidence from shallow SH-wave reflection profiles. *Seismological Research Letters*, v. 73, p. 590 – 639.

Woolery, E., Z. Wang, and R. Street (2001). Neotectonic deformation in the Fluorspar Area fault complex of western Kentucky–Evidence from shallow SH-wave reflection profiles. *Geological Society of America Annual Meeting*, Abstracts with Program, Boston, MA. T63.

## 9.0 DATA AVAILABILITY

Seismic and GPR reflection data acquired in the study were organized by site, and have been archived at the Kentucky Geological Survey as raw and processed files. In addition, there is information as to the location of the site, recording parameters, and other pertinent surveying information. The data was stored in standard SEG-Y format at the completion of the study, and is available upon request.

## 10.0 BIBLIOGRAPHY


Baker, G., 1999. Processing near-surface seismic-reflection data: A primer. Soc. of Explor. Geophy., Course Notes Series No. 9, Roger Young ed., 77 pp.

Benoit, J., 1995. Advances in pressuremeter technology with specific reference to clays. The pressuremeter and its new avenues, Proc. 4th Int. Symp. Soil Testing, 125–139.

Benoit, J., Atwood, M., Findlay, R., Hillard, B., 1995. Evaluation of jetting insertion for the self-boring pressuremeter. Can. Geotech. Jour. 32, 22–39.

Chiu, J., Johnston, A., Yang, Y., 1992. Imaging the active faults of the central New Madrid seismic zone using PANDA array data. Seism. Res. Lett. 63 (3), 375–394.

Coduto, D., 1999. Geotechnical engineering—Principles and practices. Prentice Hall, Upper Saddle River, N.J., 759 pp.

Davis, R., Lambert, T., Hanson, A., 1973. Subsurface geology and ground-water resources of the Jackson Purchase Region, Kentucky. U.S. Geol. Surv. Water Supply Pap. 1987, 47 pp.

Ellis, W., 1994. Summary and discussion of crustal stress data in the region of the New Madrid seismic zone. Investigations of the New Madrid Seismic Zone, U.S. Geol. Surv. Prof. Pap. 1538-B, 13 pp.

Hanna, A., Ghaly, A., 1992. Effects of $K_o$ and overconsolidation on uplift capacity. J. Geotech. Engineering 118 (7), 1449–1469.

Harris, J., 1996. Shear-wave splitting in Quaternary sediments: Neotectonic implications in the central New Madrid seismic zone. Geophysics 61, 1871–1882.

Harrison, R., Hoffman, D., Vaughn, J., Palmer, J., Wiscombe, C., McGeehin, J., Stephenson, W., Odum, J., Williams, R., Forman, S., 1999. An example of neotectonism in a continental interior—Thebes Gap, Midcontinent United States. Tectonophysics 305, 399–417.

Herrmann, R., Canas, J., 1978. Focal mechanism studies in the New Madrid seismic zone. Bull. Seismo. Soc. Am. 68 (4), 1095–1102.

Kolata, D., Treworgy, J., Master, J., 1981. Structural framework of the Mississippi embayment of southern Illinois. Ill. St. Geol. Surv. Circ. 516, 38 pp.

Kolata, D., Nelson, W., 1991. Tectonic history of the Illinois basin. Am. Assoc. Pet. Geol. Memoir 51, Leighton, M., Kolata, D., Oltz, D., Eidel, J., eds., 263–285.

Kulhaway, F., Beech, J., Trautmann, C., 1989. Influence of geologic development on horizontal stress in soil, *in* Foundation engineering: Current principles and practice. Am. Soc. Civ. Engineering, 43–57.

Langston, C., McIntyre, J., Street, R., Harris, J., 1998. Investigation of the shallow subsurface near the Paducah Gaseous Diffusion Plant using SH-wave seismic methods. Exp. Abs., 62nd International Meeting of the Soc. of Explor. Geophy., Sept. 13–18, New Orleans, La.

Leonards, G., Lovell, D., 1979. Interpretation of load tests on high-capacity driven piles. Behavior of Deep Foundations, ASTM STP 670, 388–415.

Mayne, P., Kulhawy, F., 1982. $K_o$-OCR relationships in soils. J. Geotech. Engineering 108, 851–872.

Mayne, P., Kulhawy, F., 1990. Direct and indirect determination of in situ $K_o$ in clays. Transp. Res. Rec. 1278, 141–149.

McBride, J., Nelson, W., 2001. Seismic reflection images of shallow faulting, northernmost Mississippi embayment, north of the New Madrid seismic zone. Bull. Seismo. Soc. Am. 91 (1), 128–139.

McBride, J., Nelson, W., Stephenson, W., 2002. Integrated geological and geophysical study of Quaternary-age deformation in the northern Mississippi embayment. Seism. Res. Lett. 73, 597–627.

Nelson, W., Lumm, D., 1987. Structural geology of southeastern Illinois and vicinity. Ill. St. Geol. Surv. Circ. 538, 70 pp.

Nelson, W., Denny, F., Devera, J., Follmer, L., Masters, J., 1997. Tertiary and Quaternary tectonic faulting in southernmost Illinois. Engineering Geol., 46, 235–258.

Nelson, W., Denny, F., Follmer, L., Masters, J., 1999. Quaternary grabens in southernmost Illinois: Deformation near an active intraplate seismic zone. Tectonophysics 305, 381–397.

Nelson, W., McBride, J., 2001. Geologic history of the northernmost Mississippi embayment and southern Illinois basin. Proc. 32nd Ann. Ohio River Valley Soils Seminar, Oct. 24, Louisville, Ky.

Olive, W., 1980. Geologic maps of the Jackson Purchase region, Kentucky. U.S. Geol. Surv. Misc. Invest. Map I-1217, 1 sheet and 11-page pamphlet.

Ross, C. , 1963. Structural framework of southernmost Illinois. Ill. St. Geol. Surv. Circ. 351, 27 pp.

Sbar, M., Sykes, L., 1973. Contemporary compressive stress and seismicity in eastern North America: An example of intra-plate tectonics. Geol. Soc. Am. Bull. 84, 1861–1882.

Schaefer, J., 2001. The influence of tectonic stress on a pile founded lock and dam. Proc. 32nd Ann. Ohio River Valley Soils Seminar, Oct. 24, Louisville, Ky.

Schwalb, H., 1969. Paleozoic geology of the Jackson Purchase region, Kentucky. Ky. Geol. Surv., Ser. 10, Rep. Invest. 10, 40 pp.

Sheriff, R., Geldart, L., 1989. Exploration seismology: History, theory, and data acquisition. Cambridge University Press, New York, 253 pp.

Stauder, W., Kramer, M., Fischer, G., Schaefer, S., Morrissey, S., 1976. Seismic characteristics of southeast Missouri as indicated by a regional telemetered microearthquake array. Bull. Seismo. Soc. Am. 66, 1953–1964.

Steeples, D., Miller, R., 1990. Seismic-reflection methods applied to engineering, environmental, and ground-water problems, Soc. of Explor. Geophy., Investigations in Geophysics no. 5, Ward, S., ed., Volume 1: Review and Tutorial, 1–30.

Turcotte, D., Ahern, J., Bird, J., 1977. The state of stress at continent margins. Tectonophysics 42, 1–28.

Wheeler, R., 1997. Boundary separating the seismically active Reelfoot Rift from the sparsely seismic Rough Creek Graben, Kentucky and Illinois. Seismo. Res. Lett. 68, 586–598.

Woolery, E., Street, R., Wang, Z., Harris, J., 1993. Near-surface deformation in the New Madrid seismic zone as imaged by high-resolution SH-wave seismic methods, Geophys. Res. Lett. 20, 1615–1618.

Woolery, E., Wang, Z., Street, R., Harris, J., 1996. A P- and SH-wave seismic investigation of the Kentucky Bend scarp in the New Madrid seismic zone. Seismo. Res. Lett. 67, 67–74.

Woolery, E., Street, R., Harris, J., Wang, Z., 1999. Neotectonic structure in the central New Madrid seismic zone: Evidence from multi-mode seismic-reflection data. Seismo. Res. Lett. 70, 554–576.

Woolery, E.W., Street, R.L., 2002. Quaternary fault reactivation in the Fluorspar Area fault complex of western Kentucky—Evidence from shallow SH-wave reflection profiles. Seismo. Res. Lett. 73, 590–639.

Woolery, E., J. Schaefer, and Z. Wang (2003). Geotechnical and geophysical indicators for local anomalous stress in the unlithified sediment of the northern Mississippi Embayment, central United States. *Tectonophysics* v.368, p. 139 – 153.

Yule, D., Sharp, M., 1988. Geophysical site investigation, Ohio River navigation project—Olmsted site. U.S. Army Corps of Engineers Misc. Pap. GL-88-15, 47 pp.

Zhu, F., Clark, J.I., 1994. The effect of dynamic loading on lateral stress in sand. Can. Geotech. Jour. 31, 308–311.

Zoback, M., 1992. First and second order pattern of stress in lithosphere: The world stress map project. J. Geophys. Res. 97, 11703–11728.

Zoback, M.L., Zoback, M.D., 1980. State of stress in conterminous United States. J. Geophys. Res. 85, 6113–6165.